Since January 2020 Elsevier has created a COVID-19 resource centre with free information in English and Mandarin on the novel coronavirus COVID-19. The COVID-19 resource centre is hosted on Elsevier Connect, the company's public news and information website.

Atmospheric Research 249 (2021) 105286

Contents lists available at ScienceDirect

Atmospheric Research

journal homepage: www.elsevier.com/locate/atmosres

Invited review article

Advances in sunphotometer-measured aerosol optical properties and related topics in China: Impetus and perspectives

Xiangao Xia[a,b,c,**], Huizheng Che[d,*], Hongrong Shi[a], Hongbin Chen[a,b,c], Xiaoye Zhang[d], Pucai Wang[a,c], Phillipe Goloub[e], Brent Holben[f]

[a] LAGEO, Institute of Atmospheric Physics, Chinese Academy of Sciences, Beijing 100029, China
[b] Collaborative Innovation Center on Forecast and Evaluation of Meteorological Disasters, Nanjing University of Information Science & Technology, Nanjing 210044, China
[c] University of Chinese Academy of Sciences, Beijing 100049, China
[d] State Key Laboratory of Severe Weather (LASW) and Key Laboratory of Atmospheric Chemistry (LAC), Chinese Academy of Meteorological Sciences, CMA, Beijing 100081, China
[e] Univ. Lille, CNRS, UMR 8518 - LOA - Laboratoire d'Optique Atmosphérique, F-59000 Lille, France
[f] Biospheric Sciences Branch, Code 923, NASA/Goddard Space Flight Center, Greenbelt, MD, USA

A B S T R A C T

Aerosol is a critical trace component of the atmosphere. Many processes in the Earth's climate system are intimately related to aerosols via their direct and indirect radiative effects. Aerosol effects are not limited to these climatic aspects, however. They are also closely related to human health, photosynthesis, new energy, etc., which makes aerosol a central focus in many research fields. A fundamental requirement for improving our understanding of the diverse aerosol effects is to accumulate high-quality aerosol data by various measurement techniques. Sunphotometer remote sensing is one of the techniques that has been playing an increasingly important role in characterizing aerosols across the world. Much progress has been made on this aspect in China during the past decade, which is the work reviewed in this paper. Three sunphotometer networks have been established to provide high-quality observations of long-term aerosol optical properties across the country. Using this valuable dataset, our understanding of spatiotemporal variability and long-term trends of aerosol optical properties has been much improved. The radiative effects of aerosols both at the bottom and at the top of the atmosphere are comprehensively assessed. Substantial warming of the atmosphere by aerosol absorption is revealed. The long-range transport of dust from the Taklimakan Desert in Northwest China and anthropogenic aerosols from South Asia to the Tibetan Plateau is characterized based on ground-based and satellite remote sensing as well as model simulations. Effective methods to estimate chemical compositions from sunphotometer aerosol products are developed. Dozens of satellite and model aerosol products are validated, shedding new light on how to improve these products. These advances improve our understanding of the critical role played by aerosols in both the climate and environment. Finally, a perspective on future research is presented.

1. Introduction

Atmospheric aerosols (aerosols hereafter) are a colloidal multiphase system composed of liquid and/or solid particles suspended in the atmosphere (Wang, 1999). Aerosols originate from both natural and anthropogenic processes. Although natural emissions are dominant in the global mean aerosol load, anthropogenic emissions are critical at regional scales and intimately linked complex effects of human activities on both climate and environment (IPCC, 2013).

Aerosol is a trace component in the atmosphere with extreme concentrations rarely exceeding a few thousand micrograms per cubic meter (Che et al., 2014). Aerosol effects on weather, climate, environment, and human health are extremely complex via the involvement with various physical and chemical processes (Li et al., 2016a, Li et al., 2016b, Li et al., 2016c; Li et al., 2017a, Li et al., 2017b, Li et al., 2017cand references therein). The Intergovernmental Panel on Climate Change (IPCC) assessment reports have repeatedly claimed that aerosol radiation effect (ARE) is one of the most uncertain factors in climate change assessment (2013). ARE is broadly defined here as aerosol effects on the radiative budget in the atmosphere, both at the bottom (BOA) and at the top of the atmosphere (TOA). ARE include aerosol absorption and scattering of solar shortwave radiation and terrestrial longwave radiation (mainly coarse-mode aerosols such as dust). Among the more important and complicated aspects of aerosols is that they act as cloud condensation nuclei, and so participate in and affect the entire life processes of cloud formation, development, and precipitation, thus indirectly affecting the energy budget of the climate system and hydrological cycle (Ramanathan et al., 2001; Kaufman et al., 2002; Li et al., 2016a, Li et al., 2016b, Li et al., 2016c). Numerous studies claim that aerosols are critical to the atmosphere, leading to a large number of

* Corresponding author.
** Corresponding author at: LAGEO, Institute of Atmospheric Physics, Chinese Academy of Sciences, Beijing 100029, China.
E-mail addresses: xxa@mail.iap.ac.cn (X. Xia), chehz@cma.gov.cn (H. Che).

https://doi.org/10.1016/j.atmosres.2020.105286
Received 19 July 2020; Received in revised form 21 September 2020; Accepted 21 September 2020
Available online 26 September 2020

important and far-reaching climatic and thereby environmental phenomena. Among these phenomena are global dimming during the period 1960–1985 and brightening since then (Wild, 2009 and references), diurnal temperature range dampening during the 1960–1980s (Wild et al., 2004; Wang and Dickinson, 2013), the pan evaporation paradox (Roderick and Farquhar, 2002; Liu et al., 2004), wind stilling (Xu et al., 2006), changes in precipitation frequency and intensity (Qian et al., 2009; Guo et al., 2016), and glacier melting over mountains (Xu et al., 2009; Qian et al., 2014; Kang et al., 2019).

Aerosols, especially those that are highly absorbing, can scatter and absorb solar radiation, leading to a decrease in surface solar radiation while heating the atmosphere of the aerosol layer, which may change the atmospheric stratification and lead to increased atmospheric stability. These processes would lead to complex feedbacks between heavily polluted weather events and ARE (Gao et al., 2015; Ding et al., 2016; Li et al., 2017a, Li et al., 2017b, Li et al., 2017c; Zheng et al., 2019; Ma et al., 2020). Furthermore, numerous studies have highlighted that the particulate matter with an aerodynamic diameter of less than 2.5 μm ($PM_{2.5}$) can directly enter the human respiratory system, thereby affecting human health and life expectancy. For example, Xie et al., 2016estimated that, in 2030, $PM_{2.5}$ pollution would cost China a 2% drop in gross domestic product and USD 25.2 billion in health expenditure.

The scattering and absorption of aerosols cause decreased direct solar radiation on the Earth's surface, while in most cases diffuse radiation to the surface increases due to aerosol scattering. Consequently, aerosols substantially alter the ratio of diffuse to direct radiation. This is a crucial subject needing thorough investigation since it involves the light use efficiency of earth ecosystems. Aerosols can also affect photosynthesis by attaching to the surface of vegetation through dry deposition (Bergin et al., 2001). In this way, aerosols also engage with the carbon cycle and affect crop yield potential. For instance, aerosols would reduce crop yield potential by 20–40% via these processes in the main grain production zone of China (Chameides et al., 1999; Tie et al., 2016; Zhang et al., 2017a, Zhang et al., 2017b). The ratio of diffuse to direct radiation is also critical in solar resource assessment and forecasting, especially for concentrating solar power generation. Dry deposition of aerosols onto solar panels also affects their solar energy absorption efficiency and temperature, which in turn affects the solar power generation efficiency (Maghami et al., 2016).

Note that our knowledge of these phenomena and their inherent processes in the Earth system is far from mature. In order to improve our understanding of the complicated aerosol effects, the first and most important foundation is to establish a solid database. We should measure not only concentration but also many other aerosol parameters, for example, particle size, absorption, and vertical distribution, to name just a few. All these aerosol properties show very large spatial and temporal variations, which pose a challenge when attempting to characterize these properties by observations. To this end, an essential part of aerosol researches is to use various measurement techniques to obtain long-term and continuous observation data of high quality. These valuable observations are essential not only for investigating how aerosol properties vary at multiple spatial and temporal scales and the internal mechanisms behind these changes, but also for examining the various aerosol effects mentioned above.

ARE is closely related to aerosol properties that can be divided into physical (including particle size, shape, etc.), chemical (composition), and optical (radiative) parameters. Aerosol optical properties include aerosol optical depth (AOD), single-scattering albedo (SSA), and phase function or asymmetry factor (all reported at 550 nm hereafter if not specified). AOD represents the column-integrated aerosol extinction coefficient. SSA and phase function represent column-integrated aerosol absorption and angular scattering distribution. Aerosol optical properties are determined by aerosol physical and chemical properties. If aerosols are assumed to be spherical, we can use the Mie scattering algorithm to calculate their optical properties, provided aerosol size distribution (number, mass, or volume concentrations varying with the particle size) and the refractive index (related to aerosol components) are known. In turn, the physical and chemical properties can be estimated from these aerosol optical properties.

Solar radiation is scattered and absorbed by various atmospheric components when it transfers through the atmosphere. On a cloudless day, atmospheric absorption from ultraviolet to infrared wavelength is mainly associated with ozone and water vapor, and the scattering process mainly refers to molecular and aerosol scattering. Since the results of these scattering and absorption processes are encoded in the surface solar spectrum or even in broadband direct and diffuse radiation, the starting point of ground-based remote sensing is to measure solar spectrum or broadband radiation. Based on the understanding of radiative transfer processes, optical, physical, and even chemical properties can then be inferred. Ground measurement of solar radiation can be traced back to the early 20th century, when the first solar constant measurement project was performed (Abbot, 1910). Handheld sunphotometer measuring only spectral direct irradiance was developed in 1950s (Volz, 1959). Automatic sunphotometer performing routine and long-term automated measurements of direct and scattered solar radiations was operated in 1990s (Nakajima et al., 1996). A thorough introduction to the history of ground-based sunpotometer remote sensing of aerosols can be found in the literature (Holben et al., 2001).

China is one of the world's major developing countries. A by-product of its population of 1.4 billion and rapid economic development during the past 40 years is a significant change in atmospheric aerosol loading and properties. China is one of the major sources of aerosols due to its vast territory and diverse topography (Luo et al., 2001; Qiu and Yang, 2000; Li et al., 2005; Li et al., 2007a; Wang et al., 2011; Zhao et al., 2020). China, especially its eastern region, can be regarded as a natural laboratory. With its complex mutual feedbacks between human activities and climate as well as environment, it provides us with a testbed for in-depth understanding of the status and role of human activities in the changes of the natural environment, and the ways in which humans and nature develop sustainably.

China has made much progress in ground-based sunphotometer remote sensing of aerosols in recent years. The aim of this paper is to present a comprehensive review of the latest advances in this field during the past 15 years (2005–2019). First, the construction and development of ground-based sunphotometer networks is introduced. Based on the valuable data from these networks, progress has been made in the following aspects: the spatiotemporal changes of aerosol optical properties; quantitative assessment of ARE; long-range transport of aerosols from neighboring regions; clarification of chemical compositions and aerosol types, and validation of satellite remote sensing and model simulation aerosol products. A perspective on possible directions for future research is presented at the end.

2. Ground-based sunphotometer remote sensing networks

Ground-based sunphotometer remote sensing of aerosols is an indispensable and accurate method to obtain column-integrated aerosol optical properties. Sunphotometer aerosol products are widely used as ground truth (although they also have certain inherent limitations) to compare and validate aerosol products from satellite remote sensing, chemical transport models, and atmospheric reanalysis. More importantly, it can provide valuable information to improve these products. Spectral direct and diffuse solar radiation from ultraviolet to near-infrared wavelengths measured by sunphotometer can be used to invert the aerosol optical, physical, and chemical properties based on the Beer–Lambert law and optimal retrieval algorithms (Holben et al., 1998; Dubovik and King, 2000; Dubovik et al., 2006).

The earliest sunphotometer observations in China started at the end of the 1970s. Zhao et al. (1983), using a self-developed handheld sunphotometer, initially revealed a distinct seasonal variation of AOD in

Beijing. Qiu et al., 1985used a modified astronomical telescope to measure direct solar radiation and forward scattering intensity of the aureole sky, and discussed the theoretical and practical feasibility of combined extinction and aureole sky radiance for the retrieval of aerosol size distribution. In terms of sunphotometer measurements at multiple sites, Zhang et al., 2002reported one-year AOD measurements at four stations by using a handheld sunphotometer, the main purpose of which was to provide ground truth for satellite remote sensing of AOD over the inland great lakes. In the spring of 2001, as an essential part of the Aerosol Characterization Experiment (ACE-Asia), four automatic sunphotometer stations were temporarily established in north China (North of 35°N) that joined the Aerosol Robotic Network (AERONET) (https://aeronet.gsfc.nasa.gov/). This campaign provided the first publicly available aerosol optical data in China. The measurements were maintained for only three months. With the support of the Sino–Japanese Dust Project at the beginning of the new century, several SKYradiometer NETwork (SKYNET) stations were established in north China, including Dunhuang, Yinchuan, Beijing, Qingdao and Hefei (Shi et al., 2005; Bi et al., 2014; Wang et al., 2014). These short-term and sporadic measurements obviously could not meet the huge demand for data from increasing aerosol researches.

Due to an abnormal occurrence of dust storms in north China at the turn of the century (Ye et al., 2000), the China Meteorological Administration established the Chinese Aerosol Research Network (CARSNET) in 2002; this was initially composed of ~20 sunphotometer stations in north China. CARSNET uses the Cimel CE-318 automatic sunphotometer as its principle instrument and follows the AERONET observation specifications and data processing protocols. Since 2010, CARSNET has been extended to include more than 60 stations across the country, which is China's largest sunphotometer network (Fig. 1). Most stations have provided continuous aerosol observation data for more than 15 years (Che et al., 2015; Che et al., 2019a). The master instrument of CARSNET is calibrated at the Izaña Observatory (Spain) in accordance with the same protocol as AERONET. The field sunphotometers are calibrated annually via the transfer of master calibration coefficients to ensure the accuracy of CARSNET (Che et al., 2009). Sky radiance is calibrated annually by using an integrating sphere in the laboratory to ensure measurement precision (Tao et al., 2014). The products include not only AOD and the Angstrom exponent (AE), a parameter quantitatively describing aerosol size, but also aerosol retrieval products from diffuse sky radiance based on the standard optimized inversion algorithm of AERONET (Dubovik et al., 2006; Xia et al., 2016; Che et al., 2019a).

In 2004, with the support of the East Asian Study of Tropospheric Aerosols: An International Regional Experiment (EAST-AIRE) (Li et al., 2007a), a nationwide handheld sunphotometer network (CSHNET) based on the Chinese Ecological Research Network (CERN) was established in 2004 (Xin et al., 2007; Wang et al., 2011). A haze meter with four wavelengths produced by the U.S. Forestry Service was initially used. It was gradually replaced by the Microtops II Sunphotometer with five wavelengths after 2010. The aerosol products mainly include AOD and AE, which, together with reflectance measurements by satellite, were used to estimate SSA (Lee et al., 2007). The network is mainly designed to validate satellite AOD products, so observations are made during the overpass time of polar orbit satellites. The instrument calibration is carried out by comparison to the AERONET sunphotometer at Xianghe (Xin et al., 2006).

The Chinese Academy of Sciences worked with a few universities to establish the Sun–Sky Radiometer Observation Network (SONET; www.sonet.ac.cn), which is initially composed of 16 stations and expands gradually. SONET uses the Cimel sunphotometer with multi-wavelength polarization measurement capability. The primary goal of the network is to provide ground truth for satellite aerosol products such as, for example, China's Gaofen series of satellites (Li et al., 2018a).

With the rapid development in sunphotometer networks, China now has three independent sunphotometer networks covering the whole country and providing long-term observation data. The data are widely used to verify satellite remote sensing retrievals, chemical model simulations, and data assimilations, to explore the spatial and temporal changes of aerosol optical characteristics, to evaluate the direct radiative effects on climate and environment of the long-range transport of aerosols, and to clarify aerosol composition and type. Publications based on these networks increased rapidly during the past decade, from several publications in 2005 to more than 150 in 2019 (Fig. 2). These results are reviewed in the following sections.

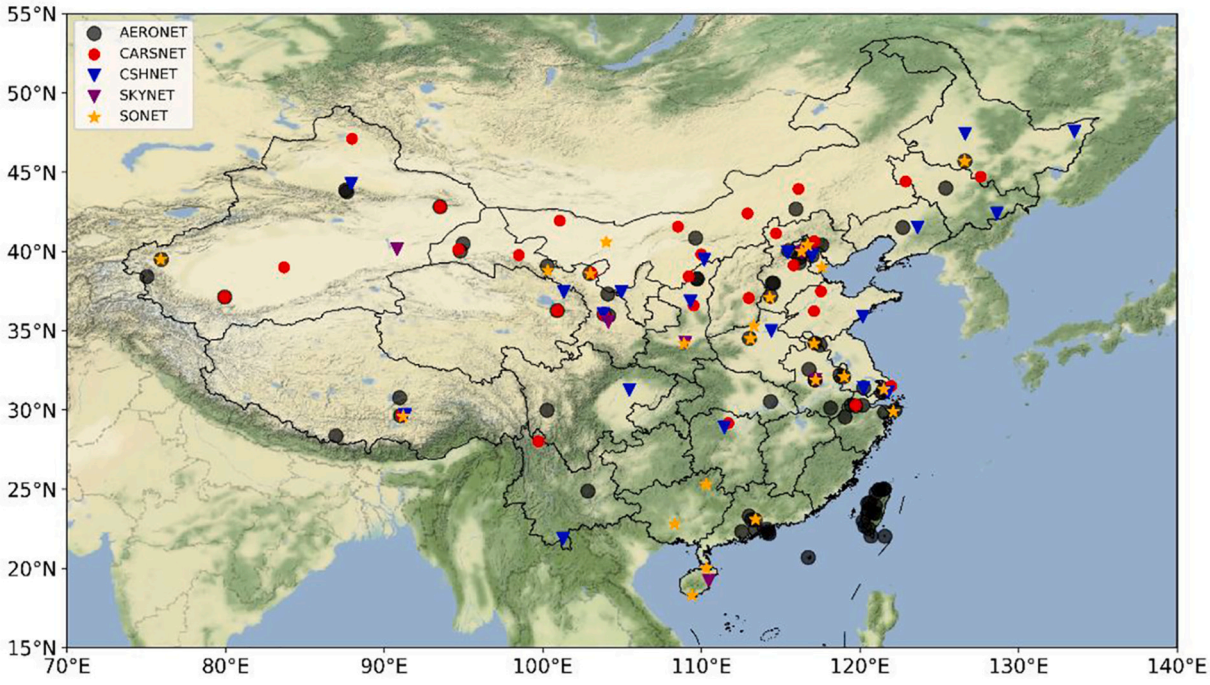

Fig. 1. Spatial distribution of sunphotometer stations from five networks, i.e., CARSNET; SONET; CSHNET; AERONET and SKYNET.

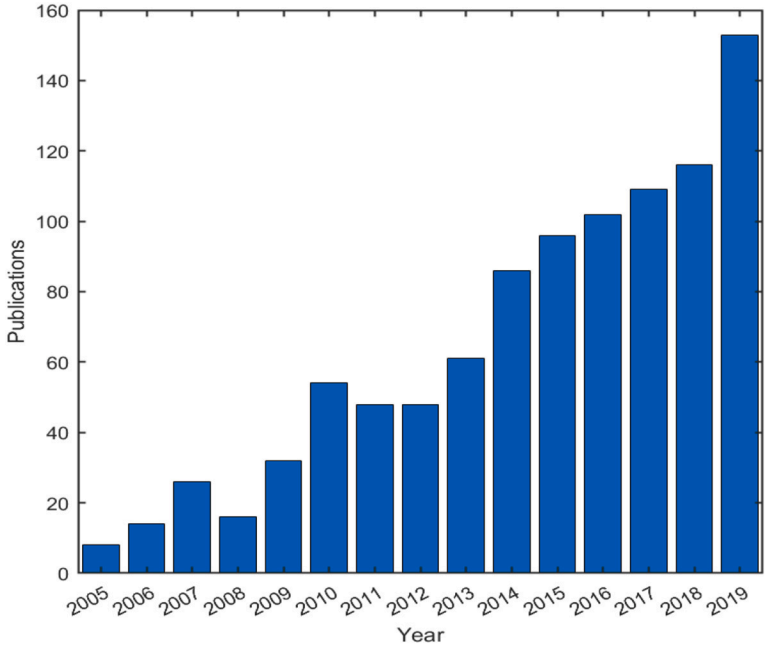

Fig. 2. Annual publications from the ISI citation web site on "AERONET + CARSNET + CSHNET + SONET + China" starting 2005.

3. Instrument calibration, retrieval algorithms, and data assessment

Regular sunphotometer calibration is fundamental to obtain high-quality measurements and thus aerosol retrieval products. Only the master sunphotometer is calibrated at high mountain stations (for instance, at Mauna Loa and Izaña) using the Langley method. The master is then used as the reference to transfer the calibration to field instruments at easily accessible sites. This is the most common method to calibrate direct-sun coefficients of sunphotometers by networks such as AERONET. On the other hand, sky radiance is commonly calibrated in the laboratory by using an integrating sphere.

Che et al. (2011) investigated the potential to establish a Langley calibration station for CARSNET at the Mt. Waliguan Observatory (100.90° E, 36.28° N, 3816 m). It was shown that the in-situ calibration coefficients differed by less than 0.5% in the infrared and visible wavelengths and 1.0% in the UV wavelengths. This indicated that the Mt. Waliguan Observatory has potential for the calibration of sunphotometers, especially in autumn and winter. Using an integrating sphere from the National Institute of Standards and Technology, U.S., a sky radiance calibration method and protocol for the CARSNET sunphotometer was established. The calibration results showed that the instrument coefficients differed by less than 3% in the visible and ~5% in the infrared wavelengths from the original calibrations by Cimel Electronique (Tao et al., 2014).

Given that regular laboratory calibration is expensive and time-consuming, alternative methods for regular calibration of sunphotometers are constantly explored. Adoption of a gain-corrected solid angle allows the interconversion of calibration coefficients derived from direct and diffuse radiation measurements, thus realizing a "vicarious" radiance calibration (Li et al., 2008). The rationale is that the CE-318 sunphotometer uses the same optical components to measure direct and diffuse radiation whereas different gains are applied. Error propagation analysis and comparison with laboratory results suggested that the uncertainty of the vicarious radiance calibration was 3–5% (Li et al., 2008).

Li et al., 2013adeveloped a novel method to transfer calibration constants from the master sunphotometer to field instruments in the laboratory. It uses an integrating sphere instead of the sun as the standard light source. The method can be applied to various types of sunphotometers because the differences in their solid viewing angle and spectral response are accounted for. A laboratory polarized light source was used to calibrate the polarization of sky radiance by the C3318-DP sunphotometer, which showed that the calibration accuracy of degree of linear polarization was about 0.005 (Li et al., 2018b).

With the development of new technologies, solar and lunar radiation can be measured by the same Cimel sun/lunar photometer (CE-318T), which makes detection of both daytime and nighttime AOD possible. Given that accurate and simple nighttime calibration is still a challenging task, Li et al., 2016a, Li et al., 2016b, Li et al., 2016cdeveloped a method to transfer a Langley calibration of direct sun radiation to nighttime measurement of lunar radiation. The transfer uncertainty was estimated to be ~2.4–2.8%.

Lee et al., 2007developed a method to estimate SSA based on a combination of spectral transmittance measurement by haze meters at the BOA and reflectance at the TOA by the Moderate Resolution Imaging Spectroradiometer (MODIS) onboard Terra and Aqua. This new method iteratively compares MODIS reflectance at the TOA with calculations by the radiative transfer model that is driven by fixed AOD and AE values from haze meters, but with varying SSA. The accuracy of SSA retrievals increased with AOD. The SSA uncertainty was estimated to within 0.02–0.03 for AOD of 1.0, which was comparable to the nominal accuracy of AERONET. The method was applied to measurements at 24 CSHNET sites. The nationwide mean SSA (at 500 nm) in 2005 was 0.89 ± 0.04.

Gui et al., 2016evaluated potential effects of external factors on measurements (for example, dust deposition on the optical head of the instrument) and therefore on AOD and AE products. It was shown that routine maintenance of sunphotometers was crucial for the accurate observation of aerosol optical properties.

Direct radiation measured by sunphotometer is contaminated by forward scattering radiance into the field-of-view (FOV) of the instrument, which may lead to systematic underestimation of AOD. Radiative transfer model simulations suggested that this effect was negligible in most cases for sunphotometers with very narrow FOV—for example, the CE-318 sunphotometer with a 1.2° FOV, the standard instrument used by CARSNET and SONET—except in the presence of heavy dust loading (Zhao et al., 2012). This argument was consistent with the conclusion by Ge et al., 2011a, Ge et al., 2011bwho showed that the error was small when the solar zenith angle was smaller than 70°.

Che et al. (2009) validated CARSNET AOD against its AERONET counterpart in Beijing. A high correlation was obtained, with the correlation coefficient (R) exceeding 0.999 and mean bias lower than 0.02. This indicates a comparable accuracy of CARSNET AOD product to that of AERONET. AERONET and SKYNET use the CE-318 sunphotometer and the PREDE skyradiometer as their major instrument, respectively. Because the two networks differ in measurement protocols and inversion algorithms, it is important to ensure that their aerosol optical properties are consistent with each other. Che et al. (2008) compared results between the two instruments in Beijing and found that the differences were < 1.3% for AOD and < 4% for SSA at wavelengths not larger than 0.67 μm. Li et al., 2018a, Li et al., 2018bshowed that the average AOD bias between SONET and AERONET was 0.002 ± 0.001, one order of magnitude smaller than the AERONET AOD uncertainty (~0.01–0.02). Jiang et al., 2020compared aerosol optical properties derived from two versions of the SKYNET retrieval package (i.e., SKYRAD.pack 5.0 and 4.2) at two sites in China. A good correlation of SSA between the two algorithms was derived, although there was a very large difference between the volume size distributions in the coarse-mode. Uncertainties in surface albedo and surface pressure produced a marginal effect on SSA retrievals.

4. Spatial and temporal changes of aerosol optical properties

Xia et al., 2005initially attempted to use aerosol data from four AERONET stations in north China in the spring of 2001 and broadband AOD retrievals from eight weather stations to study how aerosols vary spatially and temporally. Aerosol loading, size, and absorption were substantially impacted by dust activities. Alongside the rapid increase of aerosol loading due to dust activities, SSA also increased because dust absorption was lower than that of anthropogenic aerosols, especially in the near-infrared band where SSA increased from 0.84 to 0.97. Beijing and Xianghe showed coherent variation in AOD and AE, although they are about 70 km apart. R values of daily AOD and AE reached 0.99, with the magnitudes very close at the two sites, a result which was supported by analysis based on AERONET data covering more than ten years (Cong et al., 2015). This is indicative of the regional pollution in Beijing and surrounding areas. The AERONET data were also used by Cheng et al. (2006) to show how aerosol optical properties varied in East Asia. A first glance into diurnal and seasonal variation of aerosol optical characteristics was presented by Xia et al. (2006), based on 33 months of AERONET data and ground PM_{10} (particulate matter with diameter less than 10 μm) concentration data in Beijing. AOD increased gradually during daytime from early morning to late afternoon. This feature was most pronounced in winter, when AOD increased by about 5% per hour. This behavior was likely attributable to diurnal evolution of the boundary layer and the generation of secondary aerosol particles in the atmosphere. The seasonal change of AOD in Beijing was distinct. Higher AODs at 440 nm were observed in spring and summer (> 0.5) and they were relatively lower in autumn and winter (< 0.4). Surprisingly, diurnal and seasonal variations of PM_{10} were contrary to that of AOD. This demonstrated that ground and column-integrated aerosols were controlled by different processes (Qu et al., 2016).

Based on CARSNET and AERONET AOD data with more than ten years of observations at 18 sites in north China, Song et al. (2018) showed a similar daytime variation pattern in the North China Plain (NCP: 35-40° N; 110-125° E) as that in Beijing: AOD gradually increased during daytime in all four seasons, although the magnitude of the trend was seasonally dependent. A dramatically different daytime AOD variation pattern was found in northwest China (37.5-50°N, 75-110° E) relative to NCP. AOD showed a bell-shaped distribution during daytime, with relatively lower AOD in the morning and afternoon, but higher AOD around local noon. This is similar to a previous study by Wang et al. (2004), who used AOD data at Dunhuang in northwest China. Note that the dominant contribution to aerosol loading in NCP is from anthropogenic emissions, while in northwest China it is from natural processes. This is likely due to a distinctly different daytime variation of anthropogenic and natural emissions and chemical productions of aerosols in the atmosphere, which still needs further study. These diurnal variations of aerosol optical properties should be carefully accounted for in ARE estimation because it would lead to a systematic bias of up to 20% (Wang et al., 2015a, Wang et al., 2015b; Kuang et al., 2015; Xu et al., 2016; Song et al., 2018).

Human activities themselves show a weekly cycle, which may cause atmospheric pollution to exhibit its own weekly variation pattern. The term “weekend effect” was coined to describe this phenomenon. Aerosol loading during weekdays would be expected to be higher than that during the weekend because of stronger anthropogenic emissions (including traffic and industrial emissions, etc.) on working days. This was suggested to lead to an interesting weekly cycle of meteorological variables over large domains, such as temperature, precipitation, and lightening (Sanchez-Lorenzo et al., 2012 and references therein). Xia et al. (2008a, Xia et al., 2008b) initially used global AERONET data and MODIS AOD products to comprehensively study the weekly variation of AOD over global land. Weekend AOD in West Europe and the U.S. was indeed lower than AOD during weekdays. This phenomenon was more striking in urban areas. The weekly changes in AOD also accorded with religious activities in the Middle East. It was interesting to note that AOD in east China (East of 110° E) generally showed the opposite weekly change—that is, weekend AOD exceeded AOD during weekdays, which was also contrary to weekly cycling of PM_{10} (Gong et al., 2006). However, a consistent covariation of AOD and $PM_{2.5}$ was found in Shanghai by Xu et al. (2011) who argued that AOD product with coarse resolution (e.g., 1° in Xia et al., 2008a, Xia et al., 2008b) could not capture the weekly cycle at an urban scale. Song et al. (2018) used the latest MODIS Level 2 AOD product (with spatial resolution of 10 km relative to 110 km in previous studies) and $PM_{2.5}$ data to revisit this issue. The results were still similar to the previous analysis—i.e., MODIS AODs on working days were lower than weekend AODs in eastern China. This result was supported by the analysis of CARSNET and AERONET AOD products. Furthermore, the weekly variation of $PM_{2.5}$ was indeed different from that of AOD, which implied that the mechanisms determining weekly change of AOD and $PM_{2.5}$ might be different. This still requires more in-depth data analyses and numerical model simulations.

With regard to the holiday effect on aerosols, Zheng et al. (2017a, Zheng et al., 2017a) studied how spring festivals affect aerosol optical properties at three AERONET sites in NCP, and found they showed enhancement of aerosol loading and absorption during spring festival. Analysis of AOD and $PM_{2.5}$ measurements at an urban and a rural station in Beijing showed very interesting holiday components during the National Day holiday (October 1–7). Both regularly shifted from negative to positive departures, with the turning point generally occurring on October 4 (Fu et al., 2020). This is likely to be partly due to people in Beijing travelling to neighboring sites at the beginning of the holiday, causing a reduction of traffic jams in Downtown. Contrarily, high traffic inflows at the end of the holiday likely leads to increased air pollution. This hypothesis needs further model research.

Analysis of CARSNET and SONET AOD data revealed a closer look at spatial distribution of AOD and AE (Table 1) (Che et al., 2015; Li et al., 2018a, Li et al., 2018b). A revisit of spatial distribution of annual mean AOD and AE during the period of 2002-2017at CARSNET stations is shown in Fig. 3. AOD over the Tibetan Plateau and background stations in Northwest China was low (< 0.20). Industrial emissions and human activities in the Central-east China (30-35° N; 110-122° E) led to high AOD, exceeding 0.6. In the northeastern (40-55° N, 120-135° E) semi-arid and arid areas, AOD ranged from 0.20–0.40. In South China (17.5-30° N), AE exceeded 1.2, while AE was smaller than 0.8 in northwestern desert and northeastern industrial areas. Dust events in the spring, hygroscopic particle growth in the summer, seasonal biomass burning and winter heating accounted for the monthly AOD peak values,

Table 1
Annual aerosol optical properties and aerosol radiative effect (ARE, W m^{-2}) at AERONET, CARSNET and SONET stations over China. Results are mainly derived from AERONET (Xia et al., 2016), CARSNET (Che et al., 2018; Che et al., 2019b), SONET (Li et al., 2018a), CSHNET (Li et al., 2010). SKYNET results are from Wang et al. (2014). Instantaneous ARE at the solar zenith angle of ~60° (IARE) and daily mean ARE (DARE) values at the bottom (BOA) and the top of the atmosphere (TOA) are provided. AOD at 550 nm and SSA at 440 nm are presented if not specified.

Region	Site	AOD 550	AE 440-870	SSA 440	IARE BOA	IARE TOA	DARE TOA	DARE BOA	Network	Period
Northeast China	Anshan (123° E, 41.08° N, 23m)	0.58	0.79	0.89	-117.99	-39.66	/	/	CARSNET	2009-2013
	Changbai (128.63° E, 42.4° N, 736m)	0.19 ± 0.07	1.09 ± 0.44		/	/	/	-35.1	CSHNET	2004.08-2005.09
	Dalian (121.63° E, 38.9° N, 97.3m)	0.47 ± 0.08	1.22	0.93	-75.5	-37.42	/	/	CARSNET	2012-2015
	Fushun (123.95° E, 41.88° N, 80m)	0.62 ± 0.21	1.12	0.84	-116.91	-19.59	/	/	CARSNET	2009-2013
	Hailun (126.63° E, 47.43° N, 240m)	0.21 ± 0.09	1.79 ± 0.68		/	/	/	-32.3	CSHNET	2004.08-2005.09
	Harbin (126.6° E, 45.7° N, 223m)	0.33 ± 0.07	1.34 ± 0.09	0.92	/	/	-14.43	-31.1	SONET	2013.10-2016.10
	Mt.Longfeng (127.6° E, 44.73° N, 330.5m)	0.25	1.38	0.89	-51.17	-11.34	/	/	CARSNET	2012-2016
	Shenyang (123.63° E, 41.52° N, 31m)	0.46 ± 0.34	1.11 ± 0.32		/	/	/	-31.7	CSHNET	2004.08-2005.09
	Sanjiang (133.52° E, 47.58° N, 56m)	0.19 ± 0.18	1.16 ± 0.63		/	/	4.9	-36.4	CSHNET	2004.08-2005.09
	Shenyang (123.5° E, 41.77° N, 60m)	0.68 0.22	1.2	0.84	-144.88	-15.02	/	/	CARSNET	2009-2013
	Tongyu (122.92° E, 44.42° N, 182m)	0.17 0.14	1.16	0.88	-39.13	-8.87	/	/	CARSNET	2010-2011
	Tongyu (122.92° E, 44.42° N, 182m)	0.25 ± 0.27	1.11 ± 0.42	0.91 ± 0.04(550nm)	/	/	/	/	CARSNET	2010.01-2013.12
North China Plain	Beijing-IAP (116.38° E, 39.98° N, 92m)	0.62 ± 0.14	1.02 ± 0.29	0.9 ± 0.04 (550nm)	/	/			AERONET	2001.03-2012.08
	Beijing-RADI (116.3° E, 40° N, 59m)	0.61 ± 0.2	1.06 ± 0.1	0.9	/	/	-17.99	-45.95	SONET	2010.01-2016.10
	Beijing city (116.37° E, 39.97° N, 44m)	0.5 ± 0.28	1.48 ± 0.56		/	/	-6.6	-61.2	CSHNET	2004.08-2005.09
	Beijing Forest (115.43° E, 39.96° N, 1130m)	0.26 ± 0.12	0.97 ± 0.42		/	/	-3.5	-29.2	CSHNET	2004.08-2005.09
	Beijing-CAMS (116.38° E, 39.98° N, 92m)	0.5 0.11	1.12	0.9	-72.66	-29.1	/	/	CARSNET	2012-2018
	Beijing-Nanjiao (116.28° E, 39.93° N, 54.7m)	0.5 ± 0.23	1.12	0.92	-82.09	-29.43	/	/	CARSNET	2014-2017
	Datong (113.33° E, 40.1° N, 1069m)	0.44 ± 0.24	1.15	0.86	-107.86	-13.71	/	/	CARSNET	2014-2017
	Fengqiu (114.4° E, 35° N, 68m)	0.59 ± 0.21	1.09 ± 0.26		/	/	-0.2	-24.3	CSHNET	2004.08-2005.09
	Eerduosi (110.18° E, 39.48° N, 1300m)	0.24 ± 0.34	0.42 ± 0.41		/	/	0.43	-37.6	CSHNET	2004.08-2005.09
	Huimin (117.53° E, 37.5° N, 12.2m)	0.64 0.08	1.14	0.89	-111.58	-25.49	/	/	CARSNET	2009-2017
	Jiaozhou Bay (120.18° E, 35.9° N, 6m)	0.67 ± 0.3	1.11 ± 0.33		/	/	-4.2	-36	CSHNET	2004.08-2005.09
	Jiaozuo (113.25° E, 35.18° N, 113m)	0.58	1.14	0.91	-92.29	-39.35	/	/	CARSNET	2016-2017
	Shangdianzi (117.12° E, 40.65° N, 286.5m)	0.33	1.17	0.89	-59.99	-20.58	/	/	CARSNET	2014-2017
	Shijiazhuang (114.53° E, 38.03° N, 75m)	0.74	1.09	0.88	-125.05	-33.66	/	/	CARSNET	2015-2017
	Tianjin (117.17° E, 39.1° N, 5.2m)	0.64 ±	1.11	0.89	-108.09	-33.26	/	/	CARSNET	2013-2017
	Xianghe (116.96° E, 39.75° N, 36m)	0.63 ± 0.56	1.11 ± 0.29	0.91 ± 0.03(550nm)	/	/	/	/	AERONET	2001.03-2012.05
	Xilinhot (116.07° E, 43.95° N, 990.8m)	0.16	1.03	0.89	-37.14	-7.47	/	/	CARSNET	2013-2017
	Xinglong (117.58° E, 40.4° N, 970m)	0.31 ± 0.28	1.1 ± 0.31	0.94 ± 0.02(550nm)	/	/	/	/	AERONET	2001.03-2012.05
	Yushe (112.98° E, 37.07° N, 1041.8m)	0.39	1.07	0.92	-66.72	-25.99	/	/	CARSNET	2013-2017
	Zhengzhou (113.65° E, 34.72° N, 111.3m)	0.77	1.1	0.95	-101.1	-46.18	/	/	CARSNET	2013-2017
Northwest China	Akedala (87.58° E, 47.06° N, 563.3m)	0.13 ±	1.13	0.9	-0.42	-33.65	/	/	CARSNET	2013-2017
	Ansai (109.31° E, 36.85° N, 1208m)	0.38 ± 0.27	0.55 ± 0.46		/	/	-1.2	-31.8	CSHNET	2010-2017
	Dunhuang (94.68° E, 40.15° N, 1139.6m)	0.29	0.48	0.88	-8.96	-63.61	/	/	CARSNET	2012-2017
	Dunhuang (94.41° E, 40.09° N, 1140m)	0.36 ± 0.35	0.39 ± 0.22	0.9 ± 0.03(550nm)	/	/	/	/	AERONET	2011.11-2013.12
	Ejina (101.07° E, 41.95° N, 941.3m)	0.2	0.64	0.89	-47.66	-7.2	/	/	CARSNET	2013-2017
	Fukang (87.92° E, 44.28° N, 470m)	0.26 ± 0.15	0.99 ± 0.38		/	/	7.8	-22.3	CSHNET	2004.08-2005.09
	Gaolanshan (103.57° E, 36.21° N, 1668.5m)	0.3	0.81	0.89	-59.36	-20.87	/	/	CARSNET	2015-2016
	Kashi (75.9° E, 39.5° N, 1320m)	0.53 ± 0.17	0.54 ± 27	0.92	/	/	-15.72	-17.93	SONET	2013.06-2016.10
	Lanzhou (103.88° E, 36.05° N, 1518.3m)	0.55	0.81	0.83	-126.17	-13.81	/	/	CARSNET	2013-2017
	Lanzhou (103.53° E, 36.02° N, 1517m)	0.66 ± 0.28	0.82 ± 0.26	0.83 ± 0.04(550nm)	/	/	/	/	AERONET	2012.06-2013.12
	Lanzhou (103.82° E, 36.07° N, 520m)	0.69 ± 0.3	0.9 ± 0.23		/	/	/	-32.3	CSHNET	2004.08-2005.09
	Minqin (103.08° E, 38.63° N, 1368.5m)	0.25	0.68	0.86	-59.83	-5.01	/	/	CARSNET	2013-2017
	Minqin (100.3° E, 38.8° N, 1589m)	0.24 ± 0.1	0.7 ± 0.27	0.94	/	/	-9.86	-11.03	SONET	2013.01-2016.10
	SACOL (104.14° E, 35.95° N, 1965m)	0.37 ± 0.22	0.89 ± 0.27	0.92 ± 0.03(550nm)	/	/	/	/	AERONET	2006.01-2012.08
	Shapotou (104.95° E, 37.45° N, 1357m)	0.36 ± 0.13	0.71 ± 0.29		/	/	/	-20.7	CSHNET	2004.08-2005.09
	Tazhong (83.4° E, 39° N, 1099.3m)	0.56	0.25	0.92	-91.2	-23.49	/	/	CARSNET	2013-2017
	Urmqi (87.62° E, 43.78° N, 918.7m)	0.34	0.93	0.85	-70.55	-11.74	/	/	CARSNET	2012-2017
	Xi'an (108.93° E, 34.3° N, 398m)	0.78	0.98	0.88	-132.55	-35.93	/	/	CARSNET	2012-2016
	Xi'an (108.9° E, 34.2° N, 389m)	0.80 ± 0.16	1.03 ± 0.2	0.90 ± 0.04	/	/	-13.84	-33.71	SONET	2012.07-2016.10
	Yinchuan (106.22° E, 38.48° N, 1112.7m)	0.28	1.12	0.94	-48.67	-21.89	/	/	CARSNET	2017

(*continued on next page*)

Table 1 (*continued*)

Region	Site	AOD 550	AE 440-870	SSA 440	IARE BOA	IARE TOA	DARE TOA	DARE BOA	Network	Period
	Yulin (109.7° E, 38.23° N, 1058.5m)	0.26	0.84	0.89	-56.81	-9.09	/	/	CARSNET	2010-2016
	Yulin (109.72° E, 38.28° N, 1080m)	0.4 ± 0.24	0.76 ± 0.28	0.87 ± 0.04(550nm)	/	/	/	/	AERONET	2001.04-2002.10
	Zhangye (103.0° E, 38.6° N, 1364m)	0.26 ± 0.1	0.66 ± 0.2	0.94	/	/	-11.92	-13.09	SONET	2012.07-2016.10
Central-eastern China	Changde (111.7° E, 29.17° N, 565m)	0.45	1.18	0.93	-75.33	-31.44	/	/	CARSNET	2013-2016
	Chun'an (119.05° E, 29.61° N, 171.4m)	0.61	1.22	0.94	-86.49	-46.48	/	/	CARSNET	2011-2015
	Dengfeng (113.02° E, 34.46° N, 350m)	0.62	1.02	0.89	-104.78	-35.84	/	/	CARSNET	2013
	Dongtan (121.3° E, 31.4° N, 4.3m)	0.47	1.21	0.93	-79.41	-33.18	/	/	CARSNET	2012-2016
	Fuyang (119.95° E, 30.07° N, 17m)	0.66	1.31	0.94	-91.69	-42.29	/	/	CARSNET	2014-2015
	Hangzhou (119.73° E, 30.26° N, 22m)	0.68 ± 0.39	1.35 ± 0.23	0.87 ± 0.03(550nm)	/	/	/	/	AERONET	2007.08-2008.11
	Hangzhou (120.17° E, 30.23° N, 42m)	0.65	1.3	0.91	-31.57	-40.16	/	/	CARSNET	2011-2015
	Hefei (116.38° E, 31.98° N, 92m)	0.51	1.28	0.85	-105.83	-19.22	/	/	CARSNET	2016
	Hefei (116.38° E, 31.98° N, 92m)	0.63 ± 0.31	1.23 ± 0.26	0.9 ± 0.04(550nm)	/	/	/	/	AERONET	2011.01-2013.11
	Hefei (117.2° E, 31.9° N, 36m)	0.61 ± 0.09	1.2 ± 0.12	0.92	/	/	-16.05	-38	SONET	2013.01-2016.11
	Hefei (116.78° E, 31.9° N, 36m)	0.84	1.13	0.95	/	/			SKYENET	2007.03-2013.05
	Huainan (117.02° E, 32.65° N, 52m)	0.7	1.17	0.88	-129.17	-24.44	/	/	CARSNET	2014-2015
	Jiande (119.28° E, 29.45° N, 89m)	0.62	1.34	0.92	-91.06	-40.07	/	/	CARSNET	2011-2015
	Lake Tai (120.22° E, 31.4° N, 6m)	0.48 ± 0.12	0.86 ± 0.28		/	/	-5.5	-32.9	CSHNET	2004.08-2005.09
	Lin'an (119.7° E, 30.23° N, 42.6m)	0.65	1.29	0.93	-93.09	-41.73	/	/	CARSNET	2011-2015
	Nanjing (118.77° E, 32.05° N, 99.3m)	0.73	1.13	0.88	-143.38	-28.29	/	/	CARSNET	2007-2015
	Nanjing (119° E, 32.1° N, 52m)	0.63 ± 0.09	1.21 ± 0.11	0.91	/	/	-13.14	-36.81	SONET	2013.01-2016.07
	Shanghai (121.55° E, 31.22° N, 14m)	0.53	1.1	0.88	-106.89	-24.34	/	/	CARSNET	2016
	Shanghai (121.75° E, 31.13° N, 5m)	0.64 ± 0.25	1.08 ± 0.24		/	/	/	-37.9	CSHNET	2004.08-2005.09
	Shanghai (121.5° E, 31.3° N, 84m)	0.47 ± 0.12	1.26 ± 0.1	0.92	/	/	-10.26	-43.39	SONET	2013.04-2016.04
	Shouxian (116.78° E, 32.56° N, 14m)	0.74 ± 0.43	1.24 ± 0.2	0.92 ± 0.01(550nm)	/	/	/	/	AERONET	2008.05-2008.12
	Songshan (113.1° E, 34.5° N, 475m)	0.62 ± 0.13	1.12 ± 0.14	0.93	/	/	-16.11	-29.76	SONET	2013.11-2016.10
	Taihu (120.22° E, 31.42° N, 20m)	0.69 ± 0.39	1.22 ± 0.23	0.92 ± 0.03(550nm)	/	/	/	/	AERONET	2005.09-2012.10
	Taoyuan (111.45° E, 28.29° N, 78m)	0.7 ± 0.26	1.04 ± 0.23		/	/	0.5	/	CSHNET	2004.08-2005.09
	Tonglu (119.64° E, 29.8° N, 46.1m)	0.61	1.31	0.93	-89.82	-41.28	/	/	CARSNET	2011-2015
	Wuhan (114.21° E, 30.32° N, 30m)	0.77	1.16	0.88	-171.8	-20.4	/	/	CARSNET	2008
	Xiaoshan (120.25° E, 30.16° N, 14m)	0.64	1.35	0.93	-95.23	-40.39	/	/	CARSNET	2014-2015
	Zhoushan (122.1° E, 29.9° N, 29m)	0.42 ± 0.08	1.19 ± 0.05	0.95	/	/	-16.41	-29.8	SONET	2012.01-2016.10
South China	Guangzhou (113.4° E, 23.1° N, 28m)	0.63 ± 0.18	1.26 ± 0.08	9.94	/	/	-14.87	-35.19	SONET	2011.10-2016.10
	Haikou (110.3° E, 20° N, 22m)	0.41 ± 0.21	1.25 ± 0.22	0.96	/	/	-14.74	-30.25	SONET	2014.04-2016.01
	Hongkong_Hok_Tsui (114.26° E, 22.21° N, 80m)	0.39 ± 0.24	1.28 ± 0.2	0.93 ± 0.04(550nm)	/	/	/	/	AERONET	2007.11-2010.07
	Hongkong_PolyU (114.18° E, 22.3° N, 30m)	0.46 ± 0.18	1.3 ± 0.2	0.89 ± 0.02(550nm)	/	/	/	/	AERONET	2005.04-2011.10
	Hongkong_Sheung (114.12° E, 22.48° N, 40m)	0.37 ± 0.18	1.09 ± 0.21	0.88 ± 0.06(550nm)	/	/	/	/	AERONET	2012.02-2013.07
	Nanning (108.35° E, 22.82° N, 73.7m)	0.71	1.36	0.92	-121.92	-33.35	/	/	CARSNET	2013-2017
	Panyu (113.35° E, 23° N, 145m)	0.5	1.43	0.9	-96.03	-25.56	/	/	CARSNET	2012-2016
	Panyu (113.35° E, 23° N, 182m)	0.55 ± 0.23	1.27 ± 0.19	0.9 ± 0.02(550nm)	/	/	/	/	AERONET	2011.01-2013.12
	Sanya (109.4° E, 18.3° N, 29m)	0.37 ± 0.18	1.1 ± 0.23	0.94	/	/	-10.76	-30.64	SONET	2014.07-2016.10
	Xiyong (114.33° E, 22.28° N, 155.2m)	0.3	1.32	0.94	-53.18	-25.45	/	/	CARSNET	2016
	Zhuzilin (114° E, 22.32° N, 63m)	0.47	1.45	0.96	-73.16	-40.65	/	/	CARSNET	2010-2017
Southwest China	Chengdu (104.02° E, 30.67° N, 507.3m)	0.91	1.12	0.97	-110.42	-52.21	/	/	CARSNET	2014-2015
	Chengdu (104.0° E, 30.6° N, 510m)	0.82 ± 0.18	1.21 ± 0.11	0.93	/	/	-17.26	-33.19	SONET	2013.07-2016.10
	Kunming (102.65° E, 25.01° N, 1889m)	0.28 ± 0.15	1.3 ± 0.26	0.87 ± 0.03(550nm)	/	/	/	/	CARSNET	2012.04-2013.08
	Xishuangbanna (101.27° E, 21.9° N, 570m)	0.51 ± 0.24	1.47 ± 0.42		/	/	4.7	-35.62	CSHNET	2004.08-2005.09
	Yanting (105.45° E, 31.27° N, 420m)	0.9 ± 0.37	0.98 ± 0.28		/	/	1.4	-32.9	CSHNET	2004.08-2005.09
Tibetan Plateau	Haibei (101.32° E, 37.45° N, 3230m)	0.15 ± 0.07	0.9 ± 0.52		/	/	/	/	CSHNET	2004.08-2005.09
	Lhasa (91.13° E, 29.67° N, 3650.1m)	0.08	0.77	0.9	-5.04	-22.13	/	/	CARSNET	2012-2017
	Lhasa (91.33° E, 29.67° N, 3688m)	0.14 ± 0.08	0.06 ± 0.31		/	/	/	-30.6	CSHNET	2004.08-2005.09
	Lhasa (91.2° E, 29.6° N, 3678m)	0.08 ± 0.03	0.73 ± 0.08	0.84	/	/	-1.22	-1.39	SONET	2013.09-2016.10
	Mt.WLG (100.90° E, 36.28° N, 3816m)	0.12 ± 0.11	0.12 ± 0.11						AERONET	2009.09-2012.12
	NAM_CO (90.96° E, 30.77° N, 4740m)	0.04 ± 0.02	0.56 ± 0.31						AERONET	2006.08-2011.01
	QOMS_CAS (86.95° E,28.36° N, 4276m)	0.05 ± 0.29	0.94 ± 0.44						AERONET	2010.09-2012.12
	Shangrila (99.42° E, 27.5° N, 3276.7m)	0.07	1.19	0.93	-8.93	-17.43	/	/	CARSNET	2013-2017

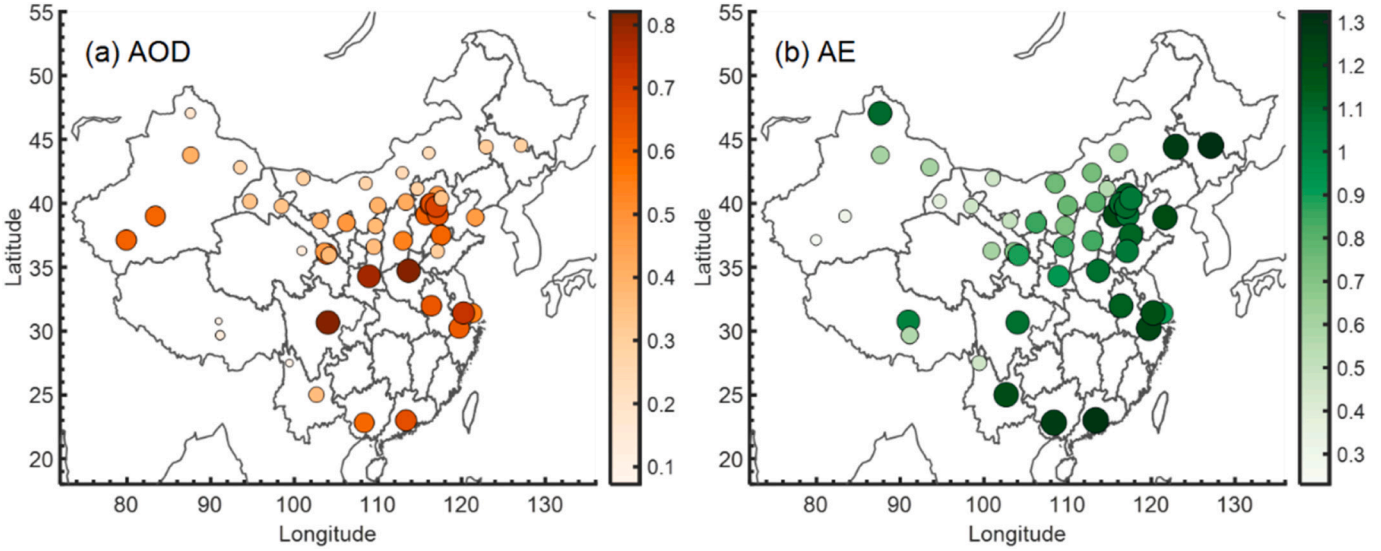

Fig. 3. A revisit spatial distribution of multi-annual mean AOD (left) and AE (right) based on CARSET and AERONET during the period of 2002-2017 in China.

especially in northern and eastern China. Detailed information about seasonal variation of AOD and AE can be found in following references (Pan et al., 2010; Wang et al., 2010; Lin et al., 2014; Wang et al., 2015a, Wang et al., 2015b; Liang et al., 2019; Qi et al., 2016; Xia et al., 2016; Li et al., 2017a, Li et al., 2017b, Li et al., 2017c; Zhao et al., 2015; Zhao et al., 2018).

Regarding the long-term AOD trend, the most important finding of Luo et al. (2001) and Qiu and Yang (2000), derived from long-term broadband solar radiation measurements at 47 stations, was that AOD in China increased from 0.38 in 1960 to 0.47 in 1990. Analysis of satellite AOD data showed an obvious upward trend of AOD from 1996–2001, and remained stable afterwards (Guo et al., 2011; Qin et al., 2018). Che et al. (2019c) used CARSNET, AERONET, MODIS, and MERRA-2 (Modern-Era Retrospective Analysis for Research and Applications, version 2) AOD products from 1980–2016 to study long-term trends at global and regional scales. AOD in East China increased up until 2010, before the trend reversed during the past decade. This agreed with the result from Qin et al. (2018), who showed that AOD increased significantly during 2000–2007 and thereafter gradually decreased from 0.297 in 2008 to 0.257 in 2017. The AOD trends derived from MERRA-2 and/or MODIS were quantitatively in agreement with CARSNET observations, which showed a decreasing trend from 2006–2009, then increasing (0.03 per year) from 2009–2013 (Che et al., 2015). AOD was observed to increase by 0.01 during 2004-2010 based CSHNET data (Xin et al., 2011). Note that more than 20 years of AOD measurements are required to obtain a statistically robust trend, given the uncertainties of measurement and autocorrelation of the AOD time series (Xia et al., 2013); therefore, long-term accurate observations are of significance.

SSA is a critical quantity in ARE. SSA at a couple of AERONET stations in China was studied by Xia et al. (2006), Cheng et al. (2006), Yu et al., 2007and Pan et al., 2010, Lee et al., 2007initially derived a nationwide mean SSA of 0.89 ± 0.04, which was associated with a large seasonal and spatial variation. For instance, at two stations in Northeast China, SSA varied from 0.75 (autumn in Hailun, 126.63° E, 47.43° N) to 0.99 (summer in Sanjiang, 133.52° E, 47.58° N). Xia et al. (2016) discussed how SSA varied spatially and temporally based on retrievals from CE-318 sunphotometer measurements at 18 stations across the country. A distinct seasonal variation of SSA was detected in East China, with generally greater SSA in summer and lower SSA in winter. Furthermore, a noticeable spatial variation of SSA at the local scale was found. This was clearly shown by a gradual increase of SSA from stations in Beijing (urban: 0.90 ± 0.04), Xianghe (suburban: 0.91 ± 0.03), and Xinglong (background: 0.94 ± 0.02) in NCP. The SSA difference between Xianghe and Beijing for the fine-mode fraction of 0.65 increased with wavelength, from ~0.02 at 440 nm to 0.06 at 1,020 nm (Eck et al., 2010). The multiyear mean SSA from 16 SONET sites varied from 0.84–0.95. Low SSA was observed in NCP and Northeast China (~0.91 in Beijing and Harbin). Aerosol absorption in coastal sites—for example, Haikou and Zhoushan—was weak, with SSA of ~0.95. SSA in Northwest China was 0.96. The overall mean SSA value calculated from these 16 stations was about 0.93 (Li et al., 2018a), which was slightly greater than found in previous studies (Lee et al., 2007; Xia et al., 2016). This is partly because of a very large spatial and temporal variation of SSA across the country, which makes mean SSAs from different stations and periods deviate from each other. Note that while SSA was reported at 550 nm in abovementioned studies, Li et al. (2018a) reported at 500 nm, which would also contribute to this spectral difference. SSA was found to increase as wavelength increases for coarse-mode dominated aerosols in Northwest China (Li et al., 2017a, Li et al., 2017b, Li et al., 2017c; Li et al., 2018a). On the other hand, SSA in the visible exceeded that in the near-infrared wavelength in East China, where anthropogenic fine aerosols are dominant. An interesting feature is that SSA at 675 nm was generally larger than that at 440 nm at many stations in East China (Li et al., 2018a), which was likely due to a moderate fraction of coarse-mode aerosols (Eck et al., 2010).

Using SSA retrievals from 50 CARSNET stations from 2010–2017, Che et al. (2019b) presented a much closer look at the spatiotemporal variability of SSA across the country than ever before. SSA at 440 nm varied from 0.88–0.97, with a nationwide mean of 0.90 ± 0.03. SSA in North China was generally less than 0.92, while in South China it exceeded 0.91. Mean SSA at urban stations was 0.90, which was slightly less than that at rural stations (0.92).

Aerosols are generally classified into types such as urban, rural, and continental, according to the features of the underlying surface. However, this classification seems too simple to generalize aerosol types in China, where we can see a dramatic difference in SSA at stations with the same underlying surface. For instance, SSA (440 nm) at four typical provincial capitals—Shengyang (Northeast China), Urumqi (Northwest China), Chengdu (Southeast China), and Hanzhou (Central-eastern China)—were 0.84, 0.85, 0.97, and 0.91, respectively (Table 1). The diversity of SSA reflects potential differences in natural and anthropogenic emissions and climate at these stations.

Few studies have focused on SSA trends because of the limited measurements. Preliminary analysis of AERONET SSA at Beijing and

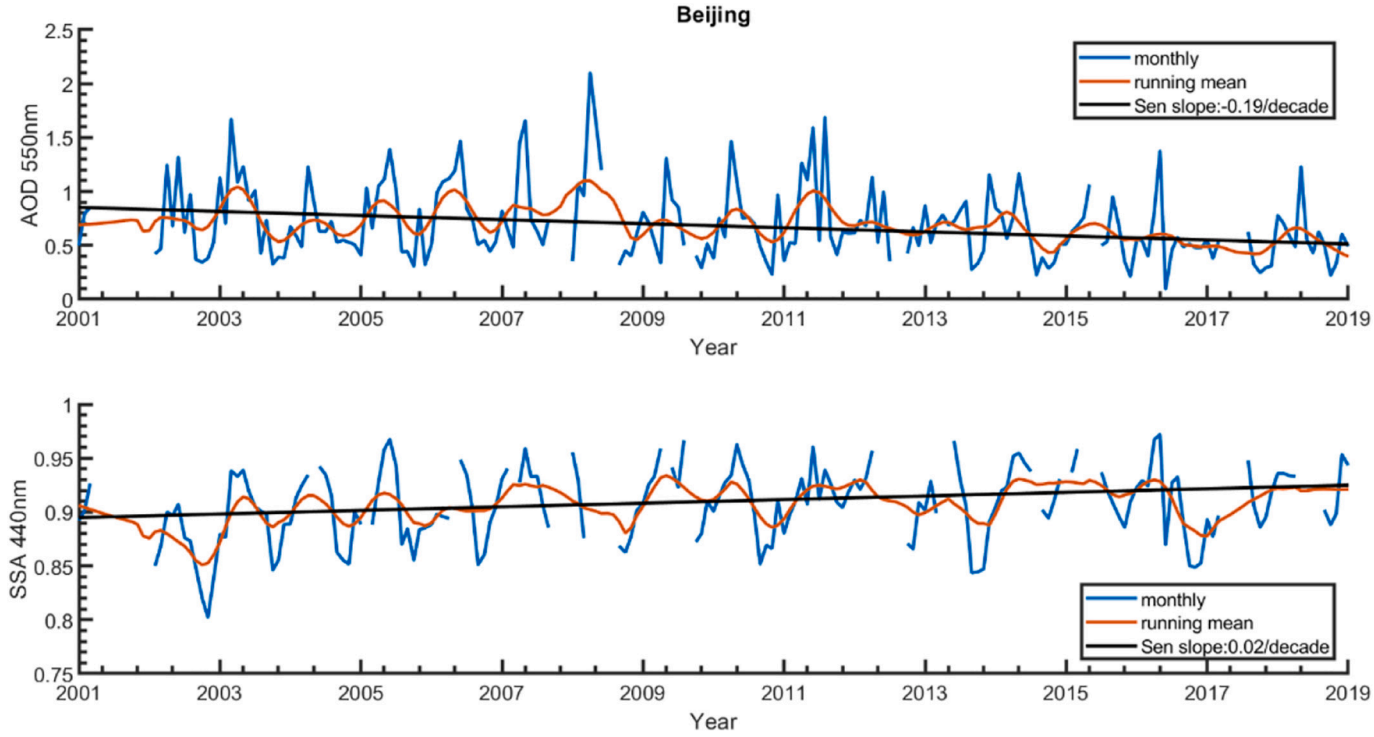

Fig. 4. Time series of monthly AERONET AOD and SSA at 440 nm and their 12-month running means in Beijing, the longest time series of ground-based remote sensing aerosol optical properties in China.

Xianghe showed an increasing trend (~0.02 during 2005–2015) (Li et al., 2018a, Li et al., 2018b). A revisited time series of monthly mean AOD and SSA at 440 nm and their 12-month running mean values in Beijing was shown in Fig. 4, which showed a decreasing rate of AOD (0.19 per decade) and an increasing rate of SSA (0.02 per decade). The increase of SSA coincided with the strict measures to control emissions of black carbon during recent years in NCP (Wang et al., 2019).

5. Assessment of aerosol direct radiative effects

Aerosol scattering and absorption lead to decreased surface solar radiation, which is closely related to issues such as crop yield, solar energy and air pollution evolution. Comprehensive observations are needed to quantify the magnitude of these effects and their relationship with aerosol optical properties. Li et al., 2007c used high-quality aerosol and radiation data from an AERONET and Baseline Surface Radiation Network (BSRN) station at Xianghe, Hebei province, and found that aerosols led to a reduction of 24 W m^{-2} in surface global solar radiation, which was comparable in magnitude to cloud radiative effect (41 W m^{-2}). This demonstrated the critical role of aerosols in the surface energy budget in this highly polluted region. Xia et al., 2007a, Xia et al., 2007bfurther studied how aerosols affected global, direct, and diffuse radiation based on AERONET aerosol and BSRN radiation data from Xianghe and Taihu. Radiative transfer model simulations were also performed to support the measurement-based analysis. A parameterization was developed to estimate ARE directly from observations. Aerosols led to a reduction of diurnal mean global solar radiation by 33 W m^{-2} at Xianghe and 38 W m^{-2} at Taihu, about half of which was accounted for by ARE in the visible spectrum. More interestingly, aerosols caused diurnal mean direct solar radiation to decrease by 90 and 113 W m^{-2} at Xianghe and Taihu, respectively, which were about three times greater in magnitude than their effect on global solar radiation. Aerosol scattering caused diffuse radiation at the two sites to increase by 51 and 67 W m^{-2}, respectively, which partly offset the reduction in direct solar radiation caused by aerosol extinction. High aerosol loading therefore not only leads to a substantial reduction in global solar radiation, but, more importantly, a dramatic decrease in the ratio of direct to diffuse radiation. Therefore, evaluation of aerosol effects on photosynthesis and thereby crop yields should thoroughly consider not only how much global solar radiation is reduced by aerosols, but also how aerosol scattering and absorption alter diffuse radiation.

Xia, 2014 further analyzed ARE associated with different aerosol types. A dramatic difference between dust and anthropogenic aerosols was found, due to their differences in particle size and absorption. Dust led to the largest ARE efficiency on direct solar radiation, but this was partly offset by strong forward scattering (i.e., dust leads to more diffuse radiation than other aerosol types). On the other hand, anthropogenic aerosols with high absorption (SSA < 0.85) were associated with a strong reduction in direct solar radiation and the largest reduction in diffuse radiation. Estimation of background surface solar radiation (in the absence of aerosols in the atmosphere) is a critical step in deriving ARE. Using global AERONET aerosol and radiation products, Xia (2015) developed a simple but effective parametrization of global solar radiation to the solar zenith angle, AOD, and water vapor. This could produce estimates of background surface solar radiation with uncertainty of 0.3 W m^{-2}, an order of magnitude lower than previous results.

Li et al. (2010) used CSHNET AOD and SSA retrievals from 25 stations across the country to drive a radiative transfer model to calculate ARE at the BOA, TOA, and in the atmosphere, which provided the first observation-based estimate of clear-sky ARE in China. The diurnal mean ARE were -15.7 ± 8.9 and 0.3 ± 1.6 W m^{-2} at the BOA and TOA, respectively. The most striking feature of the ARE was to warm up the atmosphere substantially at the expense of cooling the surface (Li et al., 2010). The fact that ARE at the TOA was marginal was mostly because of strong absorption of aerosols (nationwide mean SSA < 0.89) in the model calculation. The maximum and minimum ARE in magnitude were observed during summer and winter, respectively. The nationwide annual mean ARE efficiency (AREF)—i.e., ARE per unit AOD—was -35.1, 34.5, and -0.5 W m^{-2} at the BOA, TOA, and in the atmosphere, respectively. AREF showed a large scattering due to

spatial variation of aerosol optical properties. Specifically, AREF at the BOA varied from -20.7 ± 1.5 W m^{-2} at Shapotou (Northwest China) to -65.4 ± 4.7 W m^{-2} at Xianghe (NCP). AREF at the TOA varied from -6.6 ± 1.4 W m^{-2} at Beijing to 7.8 ± 2.1 W m^{-2} at Fukang (Northwest China). Note that AREF was derived from a linear regression of AOD to ARE at individual sites.

Based on SONET aerosol optical properties at 16 stations, average ARE at the BOA and TOA were estimated to be -28.8 ± 12.1 and -13.4 ± 4.1 W m^{-2}, respectively (Li et al., 2018a, Li et al., 2018b). This suggested that only about half of the reduction in solar radiation at the BOA was used to warm the atmosphere, which contrasted with the previous study (~100%) (Li et al., 2010). Annual mean AREF at BOA varied from -18.7 W m^{-2} at Lhasa (Tibetan Plateau) to -69.3 W m^{-2} at Shanghai. At the TOA, AREF ranged from -17.7 W m^{-2} at Minqing (Northwest China) to -29.3 W m^{-2} at Zhoushan (a coastal site in Central-eastern China). AREF was calculated as the ratio of ARE to daily mean AOD.

Note that the stations of the two networks are very different, so the substantial differences in ARE and AREF between these two studies could be partly due to spatial variation of aerosol optical properties. In particular, relatively smaller SSA retrieved by a combination of spectral transmittance and reflectance (Lee et al., 2007) as opposed to sunphotometer retrievals would account for a large part of the difference in AREF at the TOA. Aerosol warming the atmosphere but cooling the climate system was supported by many researches based on CE-318 sunphotometer measurements in East China (Table 1). For example, ARE in the atmosphere and at the TOA were 26.1 ± 5.6 and -7.3 ± 2.7 W m^{-2} in the Pearl Delta region (Mai et al., 2018), and 14.9 and -9.4 W m^{-2} in the northeastern semi-arid rural region (Wu et al., 2015). However, controversial results have been derived in Northwest China, where marginal or positive ARE at the TOA were found over desert (Huang et al., 2009; Ge et al., 2010; Ge et al., 2011a, Ge et al., 2011b; Liu et al., 2011; Bi et al., 2014; Wang et al., 2013a, Wang et al., 2013b). These studies suggested that the primary effect of dust aerosols in Northwest China was to alter the distribution of solar radiation within the climate system rather than to reflect solar energy to space. These results are due to a combination of strong absorption of aerosols (SSA < 0.9) and large surface albedo (> 0.2). Note that these results were obtained from case studies of dust events. A comprehensive analysis of AERONET aerosol optical properties at seven stations in China revealed the cooling effect of dust on the climate system. ARE at the TOA were estimated to be -15.6 W m^{-2}, about one-third of the effects at the BOA (Bi et al., 2016). SSA is a critical quantity in determining whether aerosols cool or warm the climate. Since a wide range of SSA in the visible (0.7–0.98) was found in Northwest China, this is one of the most likely reasons for the diverse ARE results at the TOA reported in the literatures.

There are also many research results on instantaneous ARE, which generally refers to ARE with the solar zenith angle of about 60°, when most AERONET retrievals are available (Table 1). Xia et al. (2016) revealed that instantaneous ARE at the BOA ranged from -66 to -111 W m^{-2} at 24 sunphotometer stations in China, which was about 3–5 times that at the TOA (from -16 to -37 W m^{-2}). SSA is the second most important parameter in determining ARE, and thus a parameterization was developed to quantify SSA effect on ARE (Xia et al., 2016). The result showed that variation of SSA by 0.01 could lead to changes of ADRE at the BOA and TOA by about 2 and 5 W m^{-2}, respectively. Che et al. (2019b) further studied instantaneous ARE based on CARSNET and AERONET data from 50 stations. ARE at the BOA increased from remote areas (-24.4 W m^{-2}) to urban areas (-103.3 W m^{-2}). At the TOA, ARE increased from -4.8 W m^{-2} at remote sites to -30.1 W m^{-2} at urban sites. Che et al., 2014; Che et al., 2018) found that, during pollution episodes in winter, ARE at the BOA exceeded -50 W m^{-2}, -180 W m^{-2}, and -200 W m^{-2} at rural, suburban, and urban sites in NCP, respectively. This result agreed with previous study undertaken in Beijing and Xianghe by Liu et al. (2007) and Wang et al. (2009a, Wang et al., 2009b), who found the instantaneous peak value of ARE at the BOA reached 350 W m^{-2}. ARE at different wavelength ranges was studied by Zhang et al. (2017a, Zhang et al., 2017b).

6. Long-range transport of aerosols from the perspective of remote sensing

Pollutants in highly polluted areas affect downwind regions on a regional scale, and even on a global scale through long-range transport (Huang et al., 2008). The Tibetan Plateau is one of the pristine areas in the world due to its high altitude and sparse population density. It is adjacent to the Taklimakan Desert in the north, the largest dust source area in East Asia (Che et al., 2013), and the Indo-Gangetic Plain in South Asia in the southwest, one of the most highly anthropogenic polluted areas across the world. The Tibetan Plateau would therefore be potentially affected by the transport of natural or anthropogenic aerosols from these surrounding source areas. Huang et al. (2007) initially revealed a dust layer aloft over northwestern Tibet (~4–7 km above sea level). Dust aerosols accumulated over the northern slopes of the Tibetan Plateau when air masses laden with Taklimakan dust moved westward, where the dust layer was eventually lofted up over the plateau. Following this study, Xia et al. (2008a, Xia et al., 2008b) used MISR AOD products to study the coherent variation of AOD over the Tibetan Plateau and the Taklimakan Desert. A good correlation was found only in summer, not in spring. This result was consistent with the argument put forward by Huang et al. (2007) that transport of Taklimakan dust would affect the Tibetan Plateau in summer.

Based on 23-months of AERONET AOD data from Lake Nam Co, a salt water lake in south central Tibet (Cong et al., 2009), Xia et al. (2011) estimated a baseline AOD of 0.029, which was lower than that over the Pacific and Atlantic islands (> 0.04). More importantly, an unusually high AOD event occurred during March 2009, with AOD as high as 0.42. Analysis of size distribution and aerosol absorption showed that this was an anthropogenic pollution event. Back-trajectory analysis revealed this pollution was very likely associated with long-range transport of anthropogenic pollution from South Asia. Further back-trajectory calculations based on a high-resolution numerical weather prediction model were used to locate the source regions and study the mechanisms of pollution transport in the complex topography of the Tibetan Plateau. A combination of synoptic-scale and local meteorological processes had enabled the lifting and advection of polluted air masses over the southern slope of the Tibetan Plateau (Lüthi et al., 2015). Data analysis and chemical model simulation of pollution events in the southern Tibetan Plateau in April and May were carried out (Zhu et al., 2019; Pokharel et al., 2019). Aerosols from biomass burning in South Asia could transport vertically to a height of 10 km, and afterwards transporting to the southern Tibetan Plateau by prevailing southwesterly winds. The central and northern Tibetan Plateau was mainly impacted by dust aerosols due to local dust events or long-range transport of dust from the Taklimakan Desert. Chemical analysis of aerosol samples from the south edge and the southeast of the plateau confirmed the findings derived from previous remote sensing and back-trajectory analyses (Cong et al., 2015; Zhao et al., 2013). The cross-Himalayan transport of polluted air masses may have far-reaching implications for the cryosphere and climate on regional to global scales. To be more specific, long-range transport of dark, light-absorbing black-carbon particles to the snow- and ice-covered mountains would exert a great melting potential on mountain cryospheric reservoirs through albedo reduction and radiative forcing. Therefore, quantifying the frequency and magnitude of the long-range transport of aerosols from South Asia to the Tibetan Plateau is highly important from a climatological perspective (Yang et al., 2014; Qian et al., 2014; Kang et al., 2019), which need a comprehensive observation strategy and in-depth model simulations.

The Yunnan–Guizhou Plateau, located in the southeast of the Tibetan Plateau, is another region in China with low aerosol

concentration. Analysis of sunphotometer aerosol properties at Kunming showed dominant aerosols from biomass during the dry season (March–April). Back-trajectory analysis revealed that airflows on polluted days mainly came from west of the site. Most biomass burning air masses originated from North Burma, where the aerosol layer could reach 5 km (Zhu et al., 2016). Model simulations showed that biomass burning in Burma and Northeast India contributed to 88% of smoke AOD at Kunming (Zhu et al., 2017).

Long-range transport of smoke aerosols from Eastern Siberia to Northeast China was evidenced by ground-based and satellite remote sensing aerosol products (Cheng et al., 2010; Li et al., 2017a, Li et al., 2017b, Li et al., 2017c). In July 2014, AOD at Tongyu, a semi-arid CARSNET site in Northeast China, experienced a dramatic increase of AOD from a background level of < 0.2 to the maximum of 2.3 during a transport event. The episode was characterized by a significant increase of fine particles and very weak absorption (SSA of 0.97, much greater than the climatological mean of 0.91) (Li et al., 2017a, Li et al., 2017b, Li et al., 2017c).

7. Chemical component retrieval and classification of aerosol types

Aerosol products from sunphotometers include not only AOD and SSA but also size distribution and its mode parameters, as well as refractive index. These parameters are largely determined by the partition of chemical components and their mixing state (Xie et al., 2014) and thus the aerosol retrieval products from AERONET, SONET, and CARSNET provide an alternative method to estimate the chemical components. Wang et al. (2013a, Wang et al., 2013b) developed a method to estimate the column-integrated contents of three major aerosol absorptive components—black carbon, brown carbon, and dust—from the spectral refractive index and SSA. The rationale behind this method lies in the distinct spectral dependence of absorption of these three components. This work was extended by Li et al. (2013b), who established a five-component model to estimate black carbon, brown carbon, dust, ammonium sulfate, and water. These components accounted respectively for 1, 2, 49, 15, and 33% of total volume of aerosols during winter haze periods in Beijing. The method of Li et al. (2013b) was further improved by Xie et al. (2016) who established a seven-component estimation method. One of the important features of this new method was that not only AOD, SSA, refractive index, and size distribution were adopted as constraints, volume fraction ratio of fine- to coarse-mode and the ratio of non-spherical to spherical particles were also used. In addition, a cost function was introduced to search for the optimal solution that made it possible to evaluate retrieval uncertainties.

Different aerosol types are characterized by distinct optical and physical properties. It is not surprising that sunphotometer aerosol products are widely used to classify aerosol types. This is one of the critical ways for the improvement of satellite remote sensing products, both passive and active. SSA (at 440 nm) and AE were widely used in the classification. Aerosols at 50 CARSNET sites were grouped into eight aerosol types that mainly differed in particle size and absorption (Che et al., 2019b). Aerosols were first classified into three types according to AE: fine-mode (AE > 1.2), mixed (0.6≤ AE < 1.2), and coarse-mode (AE < 0.6). These were then subdivided into highly, moderately, and slightly absorbing aerosols according to SSA (< 0.85, 0.85–0.95, and > 0.95). Dominant aerosol types in different regions were for the first time distinguished. Aerosols in northern China are mainly characterized by fine and coarse mixed particles with slight absorption, however, in the Central-eastern and southern China, fine mode particles are dominant and absorption is weak (Fig. 5). Satellite aerosol retrievals would benefit from such fundamental understanding of the spatial and temporal distribution of aerosol types in China.

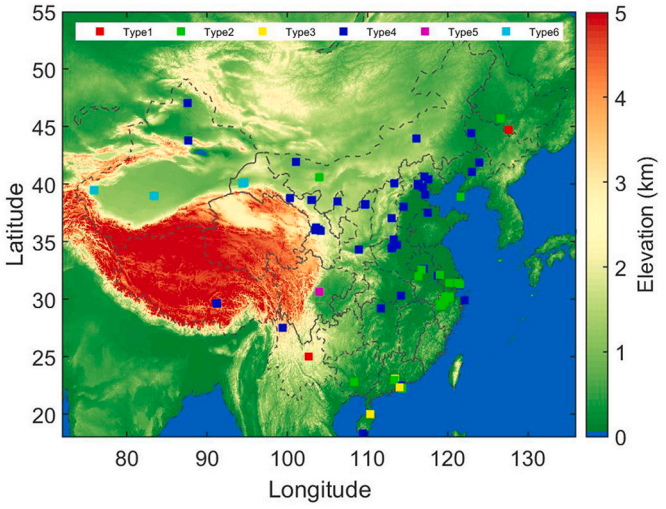

Fig. 5. Spatial distribution of the aerosol types according to multiannual mean SSA at 440 nm and AE at AERONET, CARSNET and SONET. Type1: fine mode dominate aerosols with moderate absorption (AE > 1.20, 0.85 ≤ SSA < 0.90); Type2: fine-mode dominated aerosols with slight absorption (AE > 1.20, 0.90 ≤ SSA < 0.95); Type3: fine mode dominated aerosols with weak absorption (AE > 1.20, SSA > 0.95); Type4: fine and coarse mode mixed aerosols with slight absorption (0.60 ≤ EAE < 1.20, SSA ≤ 0.95); Type5: fine and coarse mode mixed aerosols with weak absorption (0.60 ≤ EAE < 1.20, SSA > 0.95) and Type6: coarse mode dominated aerosols with slight absorption (AE ≤ 0.60, SSA ≤ 0.95).

8. Validation of satellite aerosol products

The launch of NASA's Terra satellite in December 1999 and Aqua in June 2002 was the milestone for satellite remote sensing of aerosols. The spectral and spatial resolution of MODIS and the Multi-angle Imaging SpectroRadiometer (MISR) onboard Terra represented great improvements relative to earlier instruments such as the Advanced Very High Resolution Radiometer (AVHRR). The multispectral coverage of MODIS, in particular, can provide a massive range of surface and atmospheric parameters, among which the high stability and mid-infrared band design is dedicated to satellite remote sensing of aerosols over land. Satellite remote sensing capacities have grown with further launches of spectroradiometers and lidars, to name just a few, POLDER (Polarization and Directionality of the Earth's Reflectances), a radiometer with capability to measure polarized reflectance of the atmosphere, and CALIOP (Cloud-Aerosol Lidar with Orthogonal Polarization), a space-borne lidar. Such progress in the development of aerosol retrieval algorithms, together with the launch of new imaging spectroradiometers into space, have provided aerosol products with increasing precision. Careful evaluation must be a priority in the application of these products. This is a critical step, not only to quantify the retrieval accuracy but, more importantly, to shed light on the ways to improve the retrievals.

The earlier release of MODIS AOD in inland China was less accurate than that in Europe and U.S. (Xia et al., 2004). This is likely because the aerosol optical model in the retrieval algorithm was from ground-based remote sensing products in Europe and U.S., which could not represent the real situation in China. The potential effect of MODIS cloud residuals on AOD retrievals was also examined. Validation of MODIS Collection 4 (C004) AOD products using global AERONET data showed potential impacts of surface reflectance error on spectral AOD retrievals. Specifically, up to 27% of MODIS AE values were negative, while only 1% of AERONET AE were smaller than zero. This suggested AODs at 470 nm and 660 nm should be inverted jointly, not separately (Xia et al., 2006). Mi et al. (2007) used AERONET data at Xianghe and Taihu to compare two collections of MODIS AOD products, C004 and

C005. The improved surface reflectance estimation at Xianghe and a proper choice of SSA at Taihu led to obvious improvements of C005 relative to C004. Especially in the case of low AOD levels, the accuracy of C005 was substantially improved because a fixed surface reflectance ratio of visible to mid-infrared wavelength in C004 was replaced by a dynamic parametrization. A comprehensive evaluation of C004 and C005 MODIS aerosol products against CSHNET showed that *R* increased from 0.66 (C004) to 0.84 (C005). The offset was reduced from 0.179 to 0.047 and the slope was improved from 0.74 to 0.98. However, both products tended to overestimate AOD over deserts/semi-deserts and to underestimate AOD over forests (Li et al., 2007b). The accuracy over agricultural and suburban sites exceeded that over urban areas. Xie et al. (2011) used CARSNET AOD to evaluate MODIS C005 AOD product across the country, who demonstrated that the retrieval performance was highly dependent on the underlying surface.

Che et al. (2019b) evaluated the latest Aqua MODIS C006 and C061 Dark Target (DT) 10 km AOD using sunphotometer data at 32 sites in China during 2002–2014 (CARSNET + AERONET). The performance of C061 DT was slightly better than that of C006, and the accuracy was much improved over urban surfaces in northern China. Tao et al. (2015) pointed out that MODIS Deep Blue (DB) AOD product could capture widespread haze pollution, while DT AOD was limited by its frequent missing retrievals. To be specific, more than 50% of AOD > 1.0 was missed by DT, leading to underestimation of the common regional haze pollution in eastern China. This was supported by Song et al. (2019) who found that the sampling frequency of AOD in winter by the DT algorithm was less than 30% in NCP. The advantage of DB relative to DT—i.e., remaining relatively more stable and less affected by changes in atmospheric and surface conditions—was also pointed out by Wei et al. (2019a). Validation of the MODIS Multiple Angle Implication of Atmospheric Correction (MAIAC) AOD product showed *R* of 0.94 at Xianghe and Beijing, while large deviations were generally found in other areas, and systematic underestimation was found in the desert areas of western China (Tao et al., 2019). Among the advantages of MAIAC AOD product is its capability to reveal numerous hotspots of high AOD values due to its fine spatial resolution (1 km), which makes it a good alternative in detecting $PM_{2.5}$ pollution episodes (Lyapustin et al., 2018).

The AVHRR is the only satellite sensor that has provided almost continuous global observations since 1978. Han et al. (2019) and Mei et al. (2019) took CARSNET aerosol products as the ground truth to validate AVHRR DB AOD, revealing that the accuracy of AVHRR AOD showed seasonal and spatial dependence. The AOD difference between ground and satellite products increased as sunphotometer AOD increased. Che et al. (2019a, Che et al., 2019b, Che et al., 2019c) validated AVHRR and the Along Track Scanning Radiometer (ATSR) AOD products against CARSNET data. Both products underestimated AOD and ATSR and could not provide reliable results in winter. Inter-comparison with MODIS AOD showed that AVHRR performed better than ATSR in northeastern China, while the opposite was true in southern China.

Liu et al. (2011) reported a comprehensive validation of MISR AOD product, which had, to a large extent, benefited from the establishment of CSHNET. This extended the initial validation study of MISR AOD in China by Jiang et al. (2007) who used only AERONET Beijing AOD. Although MISR AOD was well correlated to CSHNET AOD, the study found slight overestimation of AOD in the cases of relatively low AOD levels and significant underestimation of AOD in the cases of high AOD levels. In particular, MISR underestimated ~20–40% when AOD was the unit. The underestimation of MISR was likely due to weak aerosol absorption in the algorithm. SSA is generally set at 0.96, which is much higher than AERONET SSA retrievals of, for example, 0.90 in Beijing (Xia et al., 2016). As the successor to MODIS, Visible Infrared Imaging Radiometer (VIIRS) AOD product was well correlated to sunphotometer AOD with *R* of 0.91. However, the positive deviation of VIIRS AOD in spring and summer reached 0.13, a bias that increased slightly as AOD increased (Li et al., 2019). Validation of POLDER Level 2 AOD was initially carried out by Fan et al. (2008), which showed that POLDER AOD was quite consistent with AERONET AOD in terms of the fine fractional part of the size distribution (radius ≤ 0.3 μm) in northern China. Sun et al. (2010) verified this conclusion based on more AERONET data in East Asia. Further validation of the latest released POLDER aerosol products using SONET data was performed by Wei et al. (2020). The POLDER aerosol product was produced by using a statistically optimized retrieval algorithm, the core of which was the AERONET algorithm (Dubovik et al., 2011). The POLDER fine mode AOD at 490 nm was quite comparable to the SONET product with *R* of ~0.95, slope of ~0.78, and intercept of 0.07. Based on long-term AERONET data at three stations in northern China, Fan et al. (2019) systematically evaluated multiple AOD products from six space-borne imaging spectroradiometers. The latest MISR products still underestimated AOD in the case of high AOD levels. The merged DT and DB AOD product was best in terms of accuracy and sampling frequency.

Much progress has been made on the spectral and spatial resolutions of radiometers onboard geostationary satellites. The new imaging spectroradiometers— for instance, the Advanced Himawari Imager (AHI) onboard Himawari-8 in 2014, the Advanced Geosynchronous Radiation Imager (AGRI) onboard Fengyun-4, and the Advanced Baseline Imager (ABI) onboard Geostationary Operational Environmental Satellite-R (GOES-R) in 2016—share technical parameters comparable to that of MODIS. One would expect the sensors to be able to provide AOD products with quality comparable to MODIS but with a much higher frequency (5–30 minutes) during daytime. Nearly 67% of variability of sunphotometer AOD can be explained by official AHI V1.1 AOD product in China. About 55% of AHI AODs fall within the expected error range (± 0.05 ± 0.2 × AOD) (Zhang et al., 2019a, Zhang et al., 2019b). Underestimation of AHI AOD in the cases of high AOD was improved in the V2.1 version. AHI AOD in summer is the best in terms of accuracy. Results on AOD accuracy over different surface types are controversial. The best result was claimed to be achieved over urban areas by Zhang et al. (2019a, Zhang et al., 2019b), but over forest and grassland by Yang et al. (2020a). The daytime variation of AOD was captured well by AHI, but there is much space to improve the surface reflectivity parameterization and aerosol model in the algorithm (Zhang et al., 2019a, Zhang et al., 2019b; Wei et al., 2019b). By introducing the MODIS DT dynamic parameterization of surface reflection ratio, Ge et al. (2019) showed that the quality of AHI AOD was obviously improved. The R^2 between AHI and sunphotometer AODs reached 0.81.

China released many satellites for monitoring weather, climate, ocean and environment, for example, FY serious meteorological satellites (Zhang et al., 2019a, Zhang et al., 2019b). A few radiometers onboard these satellites are capable to or specified for retrieval of aerosols. AOD products from satellites such as HJ-1, FY-3 and FY-4 were validated against the counterpart from the AEORNET, CARSNET and SONET networks (Zhang et al., 2020 and references therein).

Chemical model simulations are another important source for gridded AOD products. Validation of the Georgia Tech/Goddard Global Ozone Chemistry Aerosol Radiation and Transport model (GOCART) simulation of AOD during 2001–2011 against AOD at four AERONET stations showed that only 26.8% of GOCART AODs were within ± (0.15 × AOD + 0.05) and *R* between GOCART and AERONET AODs ranged from 0.22–0.60 (Cheng et al., 2012). This indicates that the GOCART model needs further improvement in East Asia, where there is a complex mixture of aerosol sources. Song et al. (2018) indicated that MERRA-2 could capture seasonal variation of AOD, but diurnal variation of MERRA-2 disagreed with AOD and $PM_{2.5}$ measurements in NCP. Underestimation of AOD and $PM_{2.5}$ by MERRA-2 was not remedied by the assimilation of MODIS and MISR AOD products. Note that the GOCART aerosol module was used for the MERRA-2 aerosol reanalysis. Lack of nitrate simulation led to MERRA-2 underestimating AOD in the cases of high AOD, especially in winter (Song et al., 2018; Sun et al.,

2018). Assimilation of ground-based remote sensing aerosol products from networks such as CARSNET and SONET would, to some extent, overcome this deficiency.

9. Discussion and perspective

Over the past 15 years, ground-based remote sensing of aerosols by sunphotometer has made considerable progress in China. Among the most important contributions to this field was the establishment of three sunphotometer networks with good spatial coverage: CARSNET, CSHNET, and SONET. These, together with tens of AERONET stations, provide a solid data basis for aerosol research. These valuable data have been widely used in many fields. The latest progresses in sunphotometer remote sensing of aerosols in China are summarized as follows.

Understanding of the spatial and temporal changes of aerosol optical properties has been much improved. The acquisition of sunphotometer aerosol products over more than ten years provides the opportunity to study various changes in aerosol optical properties on multiple time scales. Temporal variations of aerosols, from diurnal, daily to weekly, from seasonal to inter-annual as well as decadal scales, have been revealed. AOD gradually increased during daytime in NCP, while the maximum AOD occurred at noon in northwestern China. Weekend AOD generally exceeded that on working days in eastern China, which contrasted with the weekly cycle of $PM_{2.5}$ and PM_{10}. The seasonal variations of AOD and $PM_{2.5}$ were also inconsistent in northern China. The effectiveness of measures controlling the atmospheric environment is likely reflected by the long-term evolution of aerosol optical properties, such as decreased AOD since 2010 and increased SSA in NCP. Continuous measurements are required for further analysis.

A large amount of observational evidence suggests that aerosols significantly affect surface solar radiation, not only global solar radiation but also its partition between direct and diffuse components. Using high-quality aerosol and radiation measurements, the degree of impact that aerosols have on solar radiation at the TOA, BOA, and in the atmosphere has been quantified, showing a complete picture of ARE. This lays the foundation for further study on the effects of aerosols on ecosystems, crop yield potential, and solar energy. Consistent results were obtained regarding ARE at the BOA, however, there are still some uncertainties concerning ARE at the TOA, not only in numerical value, but also in direction.

China is an important aerosol source region in East Asia. It is also affected by the long-range transport of aerosols from neighboring pollution sources. Ground-based remote sensing, combined with satellite remote sensing, back-trajectory analysis, and model simulations, showed the long-range transport of particles from biomass burning and anthropogenic pollution in South Asia to the southern slope of the Tibetan Plateau and the Yunnan–Guizhou Plateau. The transport of anthropogenic pollutants not only significantly affects the atmospheric environment over the Tibetan Plateau, but also more importantly, has a subsequent impact on high mountain glaciers and thus the Asian water cycle and climate, which merits deeper research.

Due to the scarcity of AERONET data from East Asia during the early stage of MODIS, AERONET data from Europe and U.S. were used to characterize aerosols in eastern China. This led to substantial bias in AOD retrievals. Using aerosol products from CARSNET, CSHNET, and SONET, substantial variations in aerosol optical properties were found between developed and developing countries, due to differences in their energy structures and energy use efficiency. The field of satellite remote sensing has benefited from the in-depth understanding of aerosol optical properties that came as a result of the establishment of AERONET, CARSNET, and SONET stations in China. Classification of aerosol types and analysis of aerosol chemical composition are potential areas to further promote satellite remote sensing. Preliminary validation of reanalysis aerosol products suggested that there is much space for improvement, especially in the simulation of chemical compositions.

Despite great developments in ground-based sunphotometer remote sensing of aerosols during the past decade in China, our understanding of the widespread impacts of aerosols is still far from mature, hence future work is still highly required.

More sunphotometer stations that are more evenly spaced across China are anticipated. Due to historical reasons, many more stations are located in North China than South China. Aerosols in North and South differ in their physical, chemical, and optical properties, partly due to their distinct climates. Notable differences in aerosol properties are also seen at the local scale. Therefore, it is necessary to build more stations, especially in South China.

Sunphotometer in the majority of sites is only able to measure solar radiance. A couple have been equipped with the latest sun–sky–lunar CE-318T multiband photometer, which makes measurement day and night (at full moon). Having daytime and nighttime measurements will undoubtedly provide richer information on diurnal variations of aerosol properties and then the opportunity to study their relationships to the evolution of the boundary layer and aerosol chemical production processes. Nocturnal data can also be useful for satellite remote sensing of aerosols at night, such as retrievals of AOD and $PM_{2.5}$ using VIIRS Day/Night Band measurements of artificial city lights (Fu et al., 2018). Since the lunar photometer can provide only a small amount of nighttime observations, it is necessary to develop a star photometer or to make use of starlight observations by astronomical observation instruments to enhance nocturnal aerosol measurement capabilities.

The outbreak of the coronavirus COVID-19 pandemic made the transportation of AERONET field instruments around the world extremely difficult, and greatly interfered with the regular calibration. This was a powerful reminder of the urgent need to establish a complete aerosol calibration platform and processing system in China, which would be critical for the sustainability and robustness of regional networks such as CARSNET. Inter-comparison of aerosol products between different networks is also crucial. In particular, CSHNET handheld sunphotometer calibration and data quality control procedures need to adhere to the protocols used by CARSNET and SONET. Data consistency between these independent networks is a prior requirement for their synergy.

Numerous validations of satellite aerosol products led to similar conclusions in most cases, but some controversial results were also derived. Partly, these controversies can be attributable to different data and the collocation procedures. We emphasize that the metrics for these evaluations should be considered and treated with caution. Most studies use metrics such as the root-mean-square error, mean bias, and R as the major indicators. However, it is impossible to comprehensively summarize the performance of a model by using a single indicator (Willmott, 1982). A large number of indicators with distinct statistical meaning have therefore been proposed—for example, the Kolmogorov–Smirnov test for the evaluation of accumulation distribution frequency. These new indicators could be introduced to tell a more complete story on the performance of satellite aerosol products. There would have been more attempts to use the same validation dataset to evaluate the performance of multiple satellite aerosol products, informing us quantitatively how and why the satellite products perform in this or that way. Validation studies would have been substantially enhanced if more sensitivities based on different inversion algorithms were performed (Li et al., 2009). The sensitivity studies would inform us how satellite products vary when some parts of the inversion algorithms are modified, which would then assist in providing more specific hints on how to improve satellite retrievals. Much attention should also be paid to the development and validation of satellite aerosol products based on Chinese space-borne radiometers.

Regarding ARE and AREF at the TOA, the results are still controversial. Much effort should be made to derive accurate SSA and surface albedo datasets, since these two quantities work together to determine whether aerosols cool or warm the climate system. Some areas of misunderstanding also merit mention. Surface solar radiation within 300–2,800 nm is widely calculated by radiative transfer models

to study ARE. The rationale seems to maintain consistency with solar radiation measurements. Most thermopile-based solar radiometers (pyranometers and pyrheliometers) are indeed only sensitive to solar radiation within this range of wavelength. However, they are calibrated against the absolute cavity radiometer that is sensitive to the whole spectrum of solar radiation. This means the measurements of field broadband solar radiometers have been scaled to the whole shortwave spectrum by the calibration, although with some built-in uncertainty. Although solar radiation beyond 3,200 nm is minimal, but a potential bias would be derived by this misunderstanding of solar radiation measurements. There are two methods to estimate seasonal or annual mean AREF. The first is to average daily AREF values. The second is to use the least squares regression to derive a linear relationship of daily ARE to AOD, and then to interpolate or extrapolate ARE at unit of AOD (AREF). The first method is suitable for regions with a narrow range of AOD where it is unlikely to establish a robust relationship between AOD and ARE, while the second is more suitable for situations with a wide range of AOD. Note that a slight nonlinear relationship between AOD and ARE should be treated cautiously. No matter which method is used, it is necessary to clearly state how to derive ARE and AREF, which is critical for the inter-comparison of AREF results. ARE at the TOA is generally derived by model simulations that suffer from potentially large uncertainties in input parameters and models. Direct measurement-based estimation of ARE at the TOA is required that may be achieved by the collocation of surface and satellite measurement of solar radiation (e.g., Clouds and Earth's Radiant Energy System).

There are few studies on ARE in the longwave spectrum, especially at the BOA. ARE in the longwave are expected to be weaker than in the shortwave, because AOD decreases exponentially as wavelength increases. Some special cases, for example seasonal dust events in northern China, would exert noticeable ARE in the longwave (Huang et al., 2009; Xia and Zong, 2009). This implies coarse aerosols would be potentially involved with urban heat islands via ARE in the longwave spectrum (Cao et al., 2016; Yang et al., 2020a, Yang et al., 2020b), although direct observations of ARE in the longwave are very limited. Consequently, further study of ARE in the longwave is highly anticipated.

Many measures have been taken during the past decade, especially in NCP where high-density sunphotometers have been established. The complex effects of these measures on total amount of aerosols, size, composition, absorption probably recorded by sunphotometer measurements should be carefully evaluated. Furthermore, as has been mentioned above, aerosols are a critical quantity in many research fields—ecosystem production, crop yields, solar energy assessment and forecasting, human health, among others—so much effort should also be paid to these potential influences exerted by pollution control measures.

In the past 20 years, satellite remote sensing of aerosols has made great progress. However, there is still much space for improvement. One aspect is certainly to increase satellite remote sensing information content of aerosols by using multi-wavelengths, multi-angles, and polarization remote sensing techniques. Together with rapid developments in the retrieval algorithms, one would expect much more precise satellite remote sensing aerosol products in the near future. However, it should not be overlooked that the rapid development of ground-based remote sensing networks provides opportunities to improve the accuracy and expand the spatial and temporal coverage of aerosol products by effectively merging these two products. Advanced data assimilation techniques can be used for this purpose—for example, the ensemble Kalman filter (Li et al., 2017a, Li et al., 2017b, Li et al., 2017c; Li et al., 2020).

Declaration of Competing Interest

The authors declare that they have no known competing financial interests or personal relationships that could have appeared to influence the work reported in this paper.

Acknowledgements

This work is supported by the Strategic Priority Research Program of Chinese Academy of Sciences (XDA20040501) and National Natural Science Funds of China (91644217, 42030608 and 41475138). Goloub acknowledges the support by Service National d'Observation PHOTONS/AERONET from CNRS, France AERONET-Europe ACTRIS-2 program under the European Union's Horizon 2020 research and innovation programme (654109).

References

Abbot, C., 1910. The solar constant of radiation. Smithson. Inst. Annu. Rep 319–328.
Bergin, M.H., Greenwald, R., Xu, J., Berta, Y., Chameides, W.L., 2001. Influence of aerosol dry deposition on photosynthetically active radiation available to plants: a case study in the Yangtze Delta Region of China. Geophys. Res. Lett. 28, 3605–3608.
Bi, J., Shi, J., Xie, Y., Liu, Y., Takamura, T., Khatri, P., 2014. Dust aerosol characteristics and shortwave radiative impact at a Gobi Desert of Northwest China during the Spring of 2012. J. Meteorol. Soc. Jpn. 92A, 33–56.
Bi, J., Huang, J., Hoben, B., Zhang, G., 2016. Comparison of key absorption and optical properties between pure and transported anthropogenic dust over East and Central Asia. Atmos. Chem. Phys. 16, 15501–15516.
Cao, C., Lee, X., Liu, S.D., Schultz, N., Xiao, W., Zhang, M., Zhao, L., 2016. Urban heat islands in China enhanced by haze pollution. Nat Commun. https://doi.org/10.1038/ncomms12509.
Chameides, W.L., Yu, H., Liu, S.C., Bergin, M., Zhou, X., Mearns, L., Wang, G., Kiang, C.S., Saylor, R.D., Luo, C., Huang, Y., Steiner, A., Giorgi, F., 1999. Case study of the effects of atmospheric aerosols and regional haze on agriculture: An opportunity to enhance crop yields in China through emission controls? Proc. Natl. Acad. Sci. 96, 13626–13633.
Che, H., Shi, G., Uchiyama, A., Yamazaki, A., Chen, H., Goloub, P., Zhang, X., 2008. Intercomparison between aerosol optical properties by a PREDE skyradiometer and CIMEL sunphotometer over Beijing, China. Atmos. Chem. Phys. 8, 3199–3214.
Che, H., Zhang, X., Chen, H., Damiri, B., Goloub, P., Li, Z., Zhang, X., Wei, Y., Zhou, H., Dong, F., Li, D., Zhou, T., 2009. Instrument calibration and aerosol optical depth validation of the China Aerosol Remote Sensing Network. J. Geophys. Res. 114 (D13).
Che, H., Wang, Y., Sun, J., Zhang, X., 2011. Assessment of In-situ Langley Calibration of CE-318 Sunphotometer at Mt. Waliguan Observatory, China. SOLA 7, 89–92.
Che, H., Wang, Y., Sun, J., Zhang, X., Zhang, X., Guo, J., 2013. Variation of aerosol optical properties over the taklimakan desert in China. Aerosol Air Qual. Res. 13, 777–785.
Che, H., Xia, X., Zhu, J., Li, Z., Dubovik, O., Holben, B., Goloub, P., Chen, H., Estelles, V., Cuevas-Agulló, E., Blarel, L., Wang, H., Zhao, H., Zhang, X., Wang, Y., Sun, J., Tao, R., Zhang, X., Shi, G., 2014. Column aerosol optical properties and aerosol radiative forcing during a serious haze-fog month over North China Plain in 2013 based on ground-based sunphotometer measurements. Atmos. Chem. Phys. 14, 2125–2138.
Che, H., Zhang, X.Y., Xia, X., Goloub, P., Holben, B., Zhao, H., Wang, Y., Zhang, X.C., Wang, H., Blarel, L., Damiri, B., Zhang, R., Deng, X., Ma, Y., Wang, T., Geng, F., Qi, B., Zhu, J., Yu, J., Chen, Q., Shi, G., 2015. Ground-based aerosol climatology of China: aerosol optical depths from the China Aerosol Remote Sensing Network (CARSNET) 2002–2013. Atmos. Chem. Phys. 15, 7619–7652.
Che, H., Qi, B., Zhao, H., Xia, X., Eck, T.F., Goloub, P., Dubovik, O., Estelles, V., Cuevas-Agulló, E., Blarel, L., Wu, Y., Zhu, J., Du, R., Wang, Y., Wang, H., Gui, K., Yu, J., Zheng, Y., Sun, T., Chen, Q., Shi, G., Zhang, X., 2018. Aerosol optical properties and direct radiative forcing based on measurements from the China Aerosol Remote Sensing Network (CARSNET) in eastern China. Atmos. Chem. Phys. 18, 405–425.
Che, H., Yang, L., Liu, C., Xia, X., Wang, Y., Wang, H., Wang, H., Lu, X., Zhang, X., 2019a. Long-term validation of MODIS C6 and C6.1 Dark Target aerosol products over China using CARSNET and AERONET. Chemosphere 236, 124268.
Che, H., Xia, X., Zhao, H., Dubovik, O., Holben, B.N., Goloub, P., Cuevas-Agulló, E., Estelles, V., Wang, Y., Zhu, J., Qi, B., Gong, W., Yang, H., Zhang, R., Yang, L., Chen, J., Wang, H., Zheng, Y., Gui, K., Zhang, X., Zhang, X., 2019b. Spatial distribution of aerosol microphysical and optical properties and direct radiative effect from the China Aerosol Remote Sensing Network. Atmos. Chem. Phys. 19, 11843–11864.
Che, H., Gui, K., Xia, X., Wang, Y., Holben, B.N., Goloub, P., Cuevas-Agulló, E., Wang, H., Zheng, Y., Zhao, H., Zhang, X., 2019c. Large contribution of meteorological factors to inter-decadal changes in regional aerosol optical depth. Atmos. Chem. Phys. 19, 10497–10523.
Cheng, T., Wang, H., Xu, Y., Li, H., Tian, L., 2006. Climatology of aerosol optical properties in northern China. Atmos. Environ. 40, 1495–1509.
Cheng, T., Han, Z., Zhang, R., Du, H., Jia, X., Wang, J., Yao, J., 2010. Black carbon in a continental semi-arid area of Northeast China and its possible sources of fire emission. J. Geophys. Res. 115, D23204.
Cheng, T., Chen, H., Gu, X., Yu, T., Guo, J., Guo, H., 2012. The inter-comparison of MODIS, MISR and GOCART aerosol products against AERONET data over China. J. Quant. Spectrosc. Radiat. Transfer 113, 2135–2145.
Cong, Z., Kang, S., Smirnov, A., Holben, B., 2009. Aerosol optical properties at Nam Co, a remote site in central Tibetan Plateau. Atmos. Res. 92, 42–48.
Cong, Z., Kang, S., Kawamura, K., Liu, B., Wan, X., Wang, Z., Gao, S., Fu, P., 2015.

Carbonaceous aerosols on the south edge of the Tibetan Plateau: concentrations, seasonality and sources. Atmos. Chem. Phys. 15, 1573–1584.
Ding, A., et al., 2016. Enhanced haze pollution by black carbon in megacities in China. Geophys. Res. Lett. 43, 2873–2879. https://doi.org/10.1002/2016GL067745.
Dubovik, O., King, M., 2000. A flexible inversion algorithm for retrieval of aerosol optical properties from sun and sky radiance measurements. J. Geophys. Res. 105, 20673–20696.
Dubovik, O., Sinyuk, A., Lapyonok, T., Holben, B., Mishchenko, M., Yang, P., Eck, T., Volten, H., Munoz, O., Veihelmann, B., van der Zande, W., Leon, L., Sorokin, M., Slutsker, I., 2006. Application of light scattering by spheroids for accounting for particle non-sphericity in remote sensing of desert dust. J. Geophys. Res. 111, D11208. https://doi.org/10.1029/2005JD006619.
Dubovik, O., Herman, M., Holdak, A., Lapyonok, T., Tanré, D., Deuzé, J.L., Ducos, F., Sinyuk, A., Lopatin, A., 2011. Statistically optimized inversion algorithm for enhanced retrieval of aerosol properties from spectral multi-angle polarimetric satellite observations. Atmos. Meas. Tech. 4, 975–1018.
Eck, T.F., Holben, B.N., Sinyuk, A., Pinker, R.T., Goloub, P., Chen, H., Chatenet, B., Li, Z., Singh, R.P., Tripathi, S.N., Reid, J.S., 2010. Climatological aspects of the optical properties of fine/coarse mode aerosol mixtures. J. Geophys. Res. 115, D19205. https://doi.org/10.1029/2010JD014002.
Fan, X., Goloub, P., Deuzé, J.-L., Chen, H., Zhang, W., Tanré, D., Li, Z., 2008. Evaluation of PARASOL aerosol retrieval over North East Asia. Remote Sens. Environ. 112, 697–707.
Fan, X., Xia, X.A., Chen, H., 2019. Intercomparison of Multiple Satellite Aerosol Products against AERONET over the North China Plain. Atmos 10, 480.
Fu, D., Xia, X., Wang, J., Zhang, X., Li, X., Liu, J., 2018. Synergy of AERONET and MODIS AOD products in the estimation of PM 2.5 concentrations in Beijing. Sci. Rep. 8, 1–8.
Fu, D., Song, Z., Zhang, X., Wu, Y., Duan, M., Pu, W., Ma, Z., Quan, W., Zhou, H., Che, H., Xia, X., 2020. Similarities and Differences in the Temporal Variability of PM2. 5 and AOD Between Urban and Rural Stations in Beijing. Remote Sens. 12, 1193.
Gao, Y., Zhang, M., Liu, Z., Wang, L., Wang, P., Xia, X., Tao, M., Zhu, L., 2015. Modeling the feedback between aerosol and meteorological variables in the atmospheric boundary layer during a severe fog–haze event over the North China Plain. Atmos. Chem. Phys. 15, 4279–4295.
Ge, J., Su, J., Ackerman, T.P., Fu, Q., Huang, J.P., Shi, J.S., 2010. Dust aerosol optical properties retrieval and radiative forcing over northwestern China during the 2008 China-U.S. joint field experiment. J. Geophys. Res. 115, D00K12. https://doi.org/10.1029/2009JD013263d.
Ge, J., Huang, J.P., Su, J., Bi, J.R., Fu, Q., 2011a. Shortwave radiative closure experiment and direct forcing of dust aerosol over northwestern China. Geophys. Res. Lett. 38, L24803.
Ge, J., Su, J., Fu, Q., Ackerman, T.P., Huang, J.P., 2011b. Dust aerosol forward scattering effects on ground-based aerosol optical depth retrievals. J. Quant. Spectrosc. Radiat. Transfer. 112, 310–319.
Ge, B., Li, Z., Liu, L., Yang, L., Chen, X., Hou, W., Zhang, Y., Li, D., Li, L., Qie, L., 2019. A Dark Target method for Himawari-8/AHI aerosol retrieval: application and validation. IEEE Trans. Geosci. Remote Sens. 57, 381–394.
Gong, D.Y., Guo, D., Ho, C.H., 2006. Weekend effect in diurnal temperature range in China: Opposite signals between winter and summer. J. Geophys. Res. 111, D18113.
Gui, K., et al., 2016. Analysis of the error in retrievals of aerosol optical properties from sunphotometer measurements of CARSNET due to a variety of objective factors. Atmos 7. https://doi.org/10.3390/atmos7010009.
Guo, J.P., Zhang, X.Y., Wu, Y.R., Zhaxi, Y., Che, H.Z., La, B., Wang, W., Li, X.W., 2011. Spatio-temporal variation trends of satellite-based aerosol optical depth in China during 1980–2008. Atmos. Environ. 45, 6802–6811.
Guo, J., Deng, M., Lee, S.S., Wang, F., Li, Z., Zhai, P., Liu, H., Lv, W., Yao, W., Li, X., 2016. Delaying precipitation and lightning by air pollution over the Pearl River Delta. Part I: observational analyses. J. Geophys. Res. 121, 6472–6488.
Han, X., Zou, X., Song, Z., Fu, D., Xia, X., Che, H., 2019. Comparison of AVHRR aerosol optical depth production against CARSNET data in China. Atmos. Res. 218, 12–24.
Holben, B.N., Eck, T.F., Slutsker, I.A., Tanre, D., Buis, J.P., Setzer, A., Vermote, E., Reagan, J.A., Kaufman, Y.J., Nakajima, T., Lavenu, F., 1998. AERONET - A federated instrument network and data archive for aerosol characterization. Remote Sens. Environ. 66, 1–16.
Holben, B.N., Tanre, D., Smirnov, A., Eck, T.F., Slutsker, I., Abuhassan, N., Newcomb, W.W., Schafer, J.S., Chatenet, B., Lavenu, F., Kaufman, Y.J., 2001. An emerging ground-based aerosol climatology: aerosol optical depth from AERONET. J. Geophys. Res. 106, 12067–12097.
Huang, J., Minnis, P., Yi, Y., Tang, Q., Wang, X., Hu, Y., Liu, Z., Ayers, K., Trepte, C., Winker, D., 2007. Summer dust aerosols detected from CALIPSO over the Tibetan Plateau. Geophys. Res. Lett. 34, L18805.
Huang, J., Minnis, P., Chen, B., Huang, Z., Liu, Z., Zhao, Q., Yi, Y., Ayers, J.K., 2008. Long-range transport and vertical structure of Asian dust from CALIPSO and surface measurements during PACDEX. J. Geophys. Res. 113, D23212.
Huang, J., Fu, Q., Su, J., Tang, Q., Minnis, P., Hu, Y., Yi, Y., Zhao, Q., 2009. Taklimakan dust aerosol radiative heating derived from CALIPSO observations using the Fu-Liou radiation model with CERES constraints. Atmos. Chem. Phys. 4011–4021.
IPCC, 2013. Summary for Policymakers. In: Climate Change 2013. In: The Physical Science Basis. Contribution of Working Group I to the Fifth Assessment Report of the Intergovernmental Panel on Climate Change. Cambridge University Press, Cambridge, United Kingdom and New York, NY, USA.
Jiang, X., Liu, Y., Yu, B., Jiang, M., 2007. Comparison of MISR aerosol optical thickness with AERONET measurements in Beijing metropolitan area. Remote Sens. Environ. 107, 45–53.
Jiang, Z., Duan, M., Che, H., Zhang, W., Nakajima, T., Hashimoto, M., Chen, B., Yamazaki, A., 2020. Intercomparison between the aerosol optical properties retrieved by different inversion methods from SKYNET sky radiometer observations over Qionghai and Yucheng in China. Atmos. Meas. Tech. 13, 1195–1212.
Kang, S., Zhang, Q., Qian, Y., Ji, Z., Li, C., Cong, Z., Zhang, Y., Guo, J., Du, W., Huang, J., You, Q., Panday, A.K., Rupakheti, M., Chen, D., Gustafsson, Ö., Thiemens, M.H., Qin, D., 2019. Linking atmospheric pollution to cryospheric change in the Third Pole region: current progress and future prospects. Natl. Sci. Rev. 6, 796–809.
Kaufman, Y., Tanre, D., Boucher, O., 2002. A satellite view of aerosols in the climate system. Nature. 419, 215–223.
Kuang, Y., Zhao, C.S., Tao, J.C., Ma, N., 2015. Diurnal variations of aerosol optical properties in the North China Plain and their influences on the estimates of direct aerosol radiative effect. Atmos. Chem. Phys. 15, 5761–5772.
Lee, K.H., Li, Z., Wong, M.S., Xin, J., Wang, Y., Hao, W.-M., Zhao, F., 2007. Aerosol single scattering albedo estimated across China from a combination of ground and satellite measurements. J. Geophys. Res. 112, D22S15.
Li, C., Mao, J., Lau, K., Chen, J., Yuan, Z., Liu, X., et al., 2005. Characteristics of distribution and seasonal variation of aerosol optical depth in eastern China with MODIS products. Chin. Sci. Bull. 48, 2489–2495.
Li, Z., et al., 2007a. Preface to special section on East Asian Study of Tropospheric Aerosols: an International Regional Experiment (EAST-AIRE). J. Geophys. Res. D22S00. https://doi.org/10.1029/2007JD008853.
Li, Z., Niu, F., Lee, K.-H., Xin, J., Hao, W.-M., Nordgren, B., Wang, Y., Wang, P., 2007b. Validation and understanding of Moderate Resolution Imaging Spectroradiometer aerosol products (C5) using ground-based measurements from the handheld Sun photometer network in China. J. Geophys. Res. 112, D22S07. https://doi.org/10.1029/2007JD008479.
Li, Z., Xia, X., Cribb, M., Mi, W., Holben, B., Wang, P., Chen, H., Tsay, S.C., Eck, T.F., Zhao, F., Dutton, E.G., 2007c. Aerosol optical properties and their radiative effects in northern China. J. Geophys. Res. 112 (D22).
Li, Z., Blarel, L., Podvin, T., Goloub, P., Buis, J.P., Morel, J.P., 2008. Transferring the calibration of direct solar irradiance to diffuse-sky radiance measurements for CIMEL Sun-sky radiometers. Appl. Opt. 47, 1368.
Li, Z., Zhao, X., Kahn, R., Mishchenko, M., Remer, L., Lee, K.H., et al., 2009. Uncertainties in satellite remote sensing of aerosols and impact on monitoring its long-term trend: A review and perspective. Ann. Geophys. 27, 2755–2770.
Li, Z., Lee, K.H., Wang, Y., Xin, J., Hao, W.M., 2010. First observation-based estimates of cloud-free aerosol radiative forcing across China. J. Geophys. Res. 115, D00K18.
Li, Z., Goloub, P., Blarel, L., Yang, B., Li, K., Podvin, T., Li, D., Xie, Y., Chen, X., Gu, X., Zheng, X., Li, J., Catalfamo, M., 2013a. Method to intercalibrate sunphotometer constants using an integrating sphere as a light source in the laboratory. Appl. Opt. 52, 2226.
Li, Z., Gu, X., Wang, L., Li, D., Xie, Y., Li, K., Dubovik, O., Schuster, G., Goloub, P., Zhang, Y., Li, L., Ma, Y., Xu, H., 2013b. Aerosol physical and chemical properties retrieved from ground-based remote sensing measurements during heavy haze days in Beijing winter. Atmos. Chem. Phys. 13, 10171–10183.
Li, C., Bosch, C., Kang, S., Andersson, A., Chen, P., Zhang, Q., Cong, Z., Chen, B., Qin, D., Gustafsson, Ö., 2016a. Sources of black carbon to the Himalayan–Tibetan Plateau glaciers. Nat. Commun. 7, 12574.
Li, Z., Li, K., Li, D., Yang, J., Xu, H., Goloub, P., Victori, S., 2016b. Simple transfer calibration method for a Cimel Sun–Moon photometer: calculating lunar calibration coefficients from Sun calibration constants. Appl. Opt. 55, 7624.
Li, Z., Lau, W.K.M., Ramanathan, V., Wu, G., Ding, Y., Manoj, M.G., Liu, J., Qian, Y., Li, J., Zhou, T., Fan, J., Rosenfeld, D., Ming, Y., Wang, Y., Huang, J., Wang, B., Xu, X., Lee, S.S., Cribb, M., Zhang, F., Yang, X., Zhao, C., Takemura, T., Wang, K., Xia, X., Yin, Y., Zhang, H., Guo, J., Zhai, P.M., Sugimoto, N., Babu, S.S., Brasseur, G.P., 2016c. Aerosol and monsoon climate interactions over Asia. Rev. Geophys. 54, 866–929.
Li, J., Li, X., Carlson, B.E., Kahn, R.A., Lacis, A.A., Dubovik, O., Nakajima, T., 2017a. Reducing multisensor monthly mean aerosol optical depth uncertainty: 2. Optimal locations for potential ground observation deployments. J. Geophys. Res. 122, 3920–3928. https://doi.org/10.1002/2016JD026308.
Li, X., Xia, X., Che, H., Yu, X., Liu, Y., Dubovik, O., Goloub, P., Holben, B., Estellés, V., 2017b. Contrast in column-integrated aerosol optical properties during heating and non-heating seasons at Urumqi - Its causes and implications. Atmos. Res. 191, 34–43.
Li, Z., Guo, J., Ding, A., Liao, H., Liu, J., Sun, Y., Wang, T., Xue, H., Zhang, H., Zhu, B., 2017c. Aerosols and boundary-layer interactions and impact on air quality. Natl. Sci. Rev. 4, 810–833. https://doi.org/10.1093/nsr/nwx117.
Li, Z., Li, K., Li, L., Xu, H., Xie, Y., Ma, Y., Li, D., Goloub, P., Yuan, Y., Zheng, X., 2018a. Calibration of the degree of linear polarization measurements of the polarized Sun-sky radiometer based on the POLBOX system. Appl. Opt. 57, 1011.
Li, Z., et al., 2018b. Comprehensive study of optical, physical, chemical, and radiative properties of total columnar atmospheric aerosols over China – an overview of sun-sky radiometer observation network (SONET) measurements. Bull. Ame. Meteo. Soc. https://doi.org/10.1185/BAMS-D-17-0133.1.
Li, J., Kahn, R.A., Wei, J., Carlson, B.E., Lacis, A.A., Li, Z., et al., 2020. Synergy of satellite- and ground-based aerosol optical depth measurements using an ensemble Kalman filter approach. J. Geophys. Res. 125https://doi.org/10.1029/2019JD031884. 2019JD031884.
Li, C., Li, J., Xu, H., Li, Z., Xia, X., Che, H., 2019. Evaluating VIIRS aerosol optical depth in China: an intercomparision against ground-based measurements and MODIS. J. Quan. Spec. Rad. Trans. 224, 368–377.
Liang, Y., Gui, K., Zheng, Y., Yang, X., Li, X., Liu, C., Sheng, Z., Sun, T., Zhang, X., Che, H., 2019. Impact of Biomass Burning in South and Southeast Asia on Background Aerosol in Southwest China. Aerosol Air Qual. Res. 19, 1188–1204.
Lin, J., van Donkelaar, A., Xin, J., Che, H., Wang, Y., 2014. Clear-sky aerosol optical depth over East China estimated from visibility measurements and chemical transport modeling. Atmos. Environ. 95, 258–267.
Liu, B., Xu, M., Henderson, M., Gong, W., 2004. A spatial analysis of pan evaporation

trends in China, 1955–2000. J. Geophys. Res. 109, D15102.
Liu, Y., Huang, J., Shi, G., Takamura, T., Khatri, P., Bi, J., Shi, J., Wang, T., Wang, X., Zhang, B., 2011. Aerosol optical properties and radiative effect determined from sky-radiometer over Loess Plateau of Northwest China. Atmos. Chem. Phys. 11455–11463.
Liu, J., Xia, X., Wang, P., Li, Z., Zheng, Y., Cribb, M., Chen, H., 2007. Significant aerosol direct radiative effects during a pollution episode in northern China. Geophys. Res. Lett. 34, L23808. https://doi.org/10.1029/2007GL030953.
Luo, Y., Lu, D., Zhou, X., Li, W., 2001. Characteristics of the spatial distribution and yearly variation of aerosol optical depth over China in last 30 years. J. Geophys. Res. 106, 14501–14513.
Lüthi, Z.L., Škerlak, B., Kim, S.W., Lauer, A., Mues, A., Rupakheti, M., Kang, S., 2015. Atmospheric brown clouds reach the Tibetan Plateau by crossing the Himalayas. Atmos. Chem. Phys. 15, 6007–6021.
Lyapustin, A., et al., 2018. MODIS Collection 6 MAIAC algorithm. Atmos. Meas. Tech. 11, 5741–5765.
Ma, Y., Ye, J., Xin, J., Zhang, W., 2020. The Stove, Dome, and Umbrella Effects of Atmospheric Aerosol on the Development of the Planetary Boundary Layer in Hazy Region. Geophys. Res. Lett. 47, e2020GL087373. https://doi.org/10.1029/2020GL087373.
Maghami, M.R., Hizam, H., Gomes, C., Radzi, M.A., Rezadad, M.I., Hajighorbani, S., 2016. Power loss due to soiling on solar panel: A review. Renewable Sustainable Energy Rev. 59, 1307–1316.
Mai, B., Deng, X., Li, Z., Liu, J., Xia, X.a., Che, H., Liu, X., Li, F., Zou, Y., Cribb, M., 2018. Aerosol optical properties and radiative impacts in the Pearl River Delta region of China during the dry season. Adv. Atmos. Sci. 35, 195–208.
Mei, L., Zhao, C., de Leeuw, G., Che, H., Che, Y., Rozanov, V., Vountas, M., Burrows, J.P., 2019. Understanding MODIS dark-target collection 5 and 6 aerosol data over China: Effect of surface type, aerosol loading and aerosol absorption. Atmos. Res. 228, 161–175.
Mi, W., Li, Z., Xia, X., Holben, B., Levy, R., Zhao, F., Chen, H., Cribb, M., 2007. Evaluation of the Moderate Resolution Imaging Spectroradiometer aerosol products at two Aerosol Robotic Network stations in China. J. Geophys. Res. 112, D22S08.
Nakajima, T., Tonna, G., Rao, R., Boi, P., Kaufman, Y., Holben, B., 1996. Use of sky brightness measurements from ground for remote sensing of particulate polydispersions. Appl. Opt. 35 (15), 2672–2686.
Pan, L., Che, H., Geng, F., Xia, X., Wang, Y., Zhu, C., Chen, M., Gao, W., Guo, J., 2010. Aerosol optical properties based on ground measurements over the Chinese Yangtze Delta Region. Atmos. Environ. 44, 2587–2596.
Pokharel, M., Guang, J., Liu, B., Kang, S., Ma, Y., Holben, B.N., et al., 2019. Aerosol properties over Tibetan Plateau from a decade of AERONET measurements: baseline, types, and influencing factors. J. Geophys. Res. 124, 13,357–13,374. https://doi.org/10.1029/2019JD031293.
Qi, B., Hu, D., Che, H., Du, R., Wu, Y., Xia, X., Zha, B., Liu, J., Niu, Y., Wang, H., Zhang, X., Shi, G., 2016. Seasonal Variation of Aerosol Optical Properties in an Urban Site of the Yangtze Delta Region of China. Aerosol Air Qual. Res. 16, 2884–2896.
Qian, Y., Gong, D., Fan, J., Leung, L.R., Bennartz, R., Chen, D., Wang, W., 2009. Heavy pollution suppresses light rain in China: Observations and modeling. J. Geophys. Res. 114.
Qian, Y., Yasunari, T.J., Doherty, S.J., Flanner, M.G., Lau, W.K.M., Ming, J., Wang, H., Wang, M., Warren, S.G., Zhang, R., 2014. Light-absorbing particles in snow and ice: Measurement and modeling of climatic and hydrological impact. Adv. Atmos. Sci. 32, 64–91.
Qin, W., Liu, Y., Wang, L., Lin, A., Xia, X., Che, H., Bilal, M., Zhang, M., 2018. Characteristic and driving factors of aerosol optical depth over Mainland China during 1980–2017. Remote Sens. 10, 1064.
Qiu, J.H., Yang, L.Q., 2000. Variation characteristics of atmospheric aerosol optical depths and visibility in North China during 1980–1994. Atmos. Environ. 34, 603–609.
Qiu, J., Wang, H., Zhou, X., Lu, D., 1985. Experimental study of remote sensing of atmospheric aerosol size distribution by combined solar extinction and forward scattering method. Adv. Atmos. Sci. 2, 307–315.
Qu, W., Wang, J., Zhang, X., Sheng, L., Wang, W., 2016. Opposite seasonality of the aerosol optical depth and the surface particulate matter concentration over the north China Plain. Atmos. Environ. 127, 90–99.
Ramanathan, V., Crutzen, P.J., Kiehl, J.T., Rosenfeld, D., 2001. Aerosols, climate, and the hydrological cycle. Science 294, 2119–2124.
Roderick, M.L., Farquhar, G.D., 2002. The cause of decreased pan evaporation over the past 50 years. Science 298, 1410–1411.
Sanchez-Lorenzo, A., Laux, P., Hendricks Franssen, H.J., Calbó, J., Vogl, S., Georgoulias, A.K., Quaas, J., 2012. Assessing large-scale weekly cycles in meteorological variables: a review. Atmos. Chem. Phys. 12, 5755–5771.
Shi, G., Wang, H., Wang, B., Gong, S., Zhao, T., Li, W., Aoki, T., 2005. Sensitivity experiments on the effect of optical properties of dust aerosols on their radiative forcing under clear sky condition. J. Meteo. Soc. Japan. 83A, 333e346.
Song, Z., Fu, D., Zhang, X., Wu, Y., Xia, X., He, J., Han, X., Zhang, R., Che, H., 2018. Diurnal and seasonal variability of PM2.5 and AOD in North China plain: Comparison of MERRA-2 products and ground measurements. Atmos. Environ. 191, 70–78.
Song, Z., Fu, D., Zhang, X., Han, X., Song, J., Zhang, J., Wang, J., Xia, X., 2019. MODIS AOD sampling rate and its potential effect on seasonal PM2.5 estimation in North China. Atmos. Environ 209, 14–22.
Sun, X., Goloub, P., Chiapello, I., Chen, H., Ducos, F., Li, Z., 2010. Aerosol variability over East Asia as seen by POLDER space-borne sensors. J. Geophys. Res. 115.
Sun, E., Che, H., Xu, X., Wang, Z., Lu, C., Gui, K., Zhao, H., Zheng, Y., Wang, Y., Wang, H., Sun, T., Liang, Y., Li, X., Sheng, Z., An, L., Zhang, X., Shi, G., 2018. Variation in MERRA-2 aerosol optical depth over the Yangtze River Delta from 1980 to 2016. Theor. Appl. Climatol. 136, 363–375.
Tao, R., Che, H., Chen, Q., Wang, Y., Sun, J., Zhang, X., Lu, S., Guo, J., Wang, H., Zhang, X., 2014. Development of an integrating sphere calibration method for Cimel sun-photometers in China aerosol remote sensing network. Particuology 13, 88–99.
Tao, M., Chen, L., Wang, Z., Tao, J., Che, H., Wang, X., Wang, Y., 2015. Comparison and evaluation of the MODIS Collection 6 aerosol data in China. J. Geophys. Res. 120, 6992–7005.
Tao, M., Wang, J., Li, R., Wang, L., Wang, L., Wang, Z., Tao, J., Che, H., Chen, L., 2019. Performance of MODIS high-resolution MAIAC aerosol algorithm in China: Characterization and limitation. Atmos. Environ. 213, 159–169.
Tie, X., Huang, R.J., Dai, W., Cao, J., Long, X., Su, X., Zhao, S., Wang, Q., Li, G., 2016. Effect of heavy haze and aerosol pollution on rice and wheat productions in China. Sci. Rep. 6, 29612.
Volz, F.E., 1959. Photometer mit Selen- photoelement zurspektralen Messung der Sonnenstrahlung und zer Bestimmung der Wallenlangenabhangigkeit der Dunsttrubun. Arch. Meteor.Geophys. Bioklim. B10, 100–131.
Wang, M., 1999. Atmospheric Chemistry. China Meteorological Press, Beijing.
Wang, K., Dickinson, R.E., 2013. Contribution of solar radiation to decadal temperature variability over land. Proc. Natl. Acad. Sci. 110, 14877–14882.
Wang, J., Xia, X., Wang, P., et al., 2004. Diurnal variability of dust aerosol optical thickness and Angström exponent over dust source regions in China. Geophys. Res. Lett. 31 (8). https://doi.org/10.1029/2004GL019580.
Wang, K., Dickinson, R.E., Liang, S., 2009a. Clear Sky Visibility Has Decreased over Land Globally from 1973 to 2007. Science 323, 1468–1470.
Wang, Y., Che, H., Ma, J., Wang, Q., Shi, G., Chen, H., Goloub, P., Hao, X., 2009b. Aerosol radiative forcing under clear, hazy, foggy, and dusty weather conditions over Beijing. China. Geophys. Res. Lett. 36.
Wang, P., Che, H., Zhang, X., Song, Q., Wang, Y., Zhang, Z., Dai, X., Yu, D., 2010. Aerosol optical properties of regional background atmosphere in Northeast China. Atmos. Environ. 44, 4404–4412.
Wang, Y., Xin, J., Li, Z., Wang, S., Wang, P., Hao, W.M., Nordgren, B.L., Chen, H., Wang, L., Sun, Y., 2011. Seasonal variations in aerosol optical properties over China. J. Geophys. Res. 116, D18209.
Wang, L., Li, Z., Tian, Q., Ma, Y., Zhang, F., Zhang, Y., Li, D., Li, K., Li, L., 2013a. Estimate of aerosol absorbing components of black carbon, brown carbon, and dust from ground-based remote sensing data of sun-sky radiometers. J. Geophys. Res. 118, 6534–6543.
Wang, W., Huang, J., Zhou, T., Bi, J., Lin, L., Chen, Y., Huang, Z., Su, J., 2013b. Estimation of radiative effect of a heavy dust storm over northwest China using Fu-Liou model and ground measurements. J. Quan. Spec. Rad. Tran. 122, 114–126.
Wang, Z., Liu, D., Wang, Z., Wang, Y., kHATRI, p., Zhou, J., Takamura, T., Shi, G., 2014. Seasonal characterisitics of aerosol optical properties at the SKYNET Hefei site (31.90 N, 117.17 E) from 2007 to 2013. JJ. Geophys. Res. https://doi.org/10.1002/2014JD021500.
Wang, L., Gong, W., Xia, X., Zhu, J., Li, J., Zhu, Z., 2015a. Long-term observations of aerosol optical properties at Wuhan, an urban site in Central China. Atmos. Environ. 101, 94–102.
Wang, Z., Liu, D., Wang, Y., et al., 2015b. Diurnal aerosol variations do affect daily averaged radiative forcing under heavy aerosol loading observed in Hefei. China. Atmos. Meas. Tech. 8, 2901–2907.
Wang, Y., Li, W., Gao, W., Liu, Z., Tian, S., Shen, R., Ji, D., Wang, S., Wang, L., Tang, G., Song, T., 2019. Trends in particulate matter and its chemical compositions in China from 2013–2017. Science China Earth Sciences 62, 1857–1871.
Wei, J., Li, Z., Peng, Y., Sun, L., 2019a. MODIS Collection 6.1 aerosol optical depth products over land and ocean: validation and comparison. Atmos. Environ. 201, 428–440. https://doi.org/10.1016/j.atmosenv.2018.12.004.
Wei, J., Li, Z., Sun, L., Peng, Y., Zhang, Z., Li, Z., Su, T., Feng, L., Cai, Z., Wu, H., 2019b. Evaluation and uncertainty estimate of next-generation geostationary meteorological Himawari-8/AHI aerosol products. Sci. Total Environ. 692, 879–891.
Wei, Y., Li, Z., Zhang, Y., Chen, C., Dubovik, O., Zhang, Y., Xu, H., Li, K., Chen, J., Wang, H., Ge, B., Fan, C., 2020. Validation of POLDER GRASP aerosol optical retrieval over China using SONET observations. J. Quant. Spectrosc. Radiat. Transfer 246, 106931.
Wild, M., 2009. Global dimming and brightening: A review. J. Geophys. Res. 114 (D10).
Wild, M., Ohmura, A., Gilgen, H., Rosenfeld, D., 2004. On the consistency of trends in radiation and temperature records and implications for the global hydrological cycle. Geophys. Res. Lett. 31, L11201.
Willmott, C., 1982. Some comments on the evaluation of model performance. Bull. Am. Meteorol. Soc. 11, 1309–1313.
Wu, Y., Zhu, J., Che, H., Xia, X., Zhang, R., 2015. Column-integrated aerosol optical properties and direct radiative forcing based on sun photometer measurements at a semi-arid rural site in Northeast China. Atmos. Res. 157, 56–65.
Xia, X., 2014. A critical assessment of direct radiative effects of different aerosol types on surface global radiation and its components. J. Quan. Spect. Rad. Trans. 149, 72–80.
Xia, X., 2015. Parameterization of clear-sky surface irradiance and its implications for estimation of aerosol direct radiative effect and aerosol optical depth. Sci. Rep. 5, 14376. https://doi.org/10.1038/srep14376.
Xia, X., Zong, X., 2009. Shortwave versus longwave direct radiative forcing by Taklimakan dust aerosols. Geophys. Res. Lett. 36, L07803.
Xia, X., Chen, H., Wang, P., 2004. Validation of MODIS aerosol retrievals and evaluation of potential cloud contamination in East Asia. J. Environ. Sci. 5, 832–837.
Xia, X., Chen, H., Wang, P., Zong, X., Qiu, J., Goloub, P., 2005. Aerosol properties and their spatial and temporal variations over North China in spring 2001. Tellus 57B, 28–39.
Xia, X., Chen, H., Wang, P., Zhang, W., Goloub, P., Chatenet, B., Eck, T., Holben, B., 2006. Variation of column-integrated aerosol properties in a Chinese urban region. J. Geophys. Res. 111, D05204.

Xia, X., Li, Z., Wang, P., Chen, H., Cribb, M., 2007a. Estimation of aerosol effects on surface irradiance based on measurements and radiative transfer model simulations in northern China. J. Geophys. Res. 112, D22S10.
Xia, X., Li, Z., Holben, B., Wang, P., Eck, T., Chen, H., Cribb, M., Zhao, Y., 2007b. Aerosol optical properties and radiative effects in the Yangtze Delta region of China. J. Geophys. Res. 112, D22S12.
Xia, X., Wang, P., Wang, Y., Li, Z., Xin, J., Liu, J., Chen, H., 2008a. Aerosol optical depth over the Tibetan Plateau and its relation to aerosols over the Taklimakan Desert. Geophys. Res. Lett. 35, L16804.
Xia, X., Eck, T.F., Holben, B.N., Phillippe, G., Chen, H., 2008b. Analysis of the weekly cycle of aerosol optical depth using AERONET and MODIS data. J. Geophys. Res. 113, D14217.
Xia, X., Zong, X., Cong, Z., Chen, H., Kang, S., Wang, P., 2011. Baseline continental aerosol over the central Tibetan plateau and a case study of aerosol transport from South Asia. Atmos. Environ. 45, 7370–7378.
Xia, X., Chen, H., Goloub, P., Zong, X., Zhang, W., Wang, P., 2013. Climatological aspects of aerosol optical properties in North China based on ground and satellite remote-sensing data. J. Quan. Spect. Rad. Trans. 127, 12–23.
Xia, X., Che, H., Zhu, J., Chen, H., Cong, Z., Deng, X., Fan, X., Fu, Y., Goloub, P., Jiang, H., Liu, Q., Mai, B., Wang, P., Wu, Y., Zhang, J., Zhang, R., Zhang, X., 2016. Ground-based remote sensing of aerosol climatology in China: Aerosol optical properties, direct radiative effect and its parameterization. Atmos. Environ. 124, 243–251.
Xie, Y., Zhang, Y., Xiong, X., Qu, J.J., Che, H., 2011. Validation of MODIS aerosol optical depth product over China using CARSNET measurements. Atmos. Environ. 45, 5970–5978.
Xie, Y., Li, Z., Li, L., Wang, L., Li, D., Chen, C., Li, K., Xu, H., 2014. Study on influence of different mixing rules on the aerosol components retrieval from ground-based remote sensing measurements. Atmos. Res. 145-146, 267–278.
Xie, Y., Dai, H., Dong, H., Hanaoka, T., Masui, T., 2016. Economic impacts from $PM_{2.5}$ pollution-related health effects in China: a provincial-level analysis. Environ. Sci. Technol. 50, 4836–4843.
Xin, J., Wang, Y., Li, Z., Wang, P., Wang, S., Wen, T., Sun, Y., 2006. Introduction and calibration of the Chinese Sun Hazemeter Network. Environ. Sci. 27, 1697–1702.
Xin, J., Wang, Y., Li, Z., Wang, P., Hao, W.M., Nordgren, B.L., Wang, S., Liu, G., Wang, L., Wen, T., Sun, Y., Hu, B., 2007. Aerosol optical depth (AOD) and Ångström exponent of aerosols observed by the Chinese Sun Hazemeter Network from August 2004 to September 2005. J. Geophys. Res. 112, D05203.
Xin, J., Wang, L., Wang, Y., Li, Z., Wang, P., 2011. Trends in aerosol optical properties over the Bohai Rim in Northeast China from 2004 to 2010. Atmos. Environ. 45, 6317–6325.
Xu, M., et al., 2006. Steady decline of East Asian monsoon winds, 1969–2000: evidence from direct ground measurements of wind speed. J. Geophys. Res. 111, D24111. https://doi.org/10.1029/2006JD007337.
Xu, B., Cao, J., Hansen, J., Yao, T., Joswia, D.R., Wang, N., Wu, G., Wang, M., Zhao, H., Yang, W., Liu, X., He, J., 2009. Black soot and the survival of Tibetan glaciers. Proc. Natl. Acad. Sci. 106, 22114–22118.
Xu, J., Li, C., Shi, H., He, Q., Pan, L., 2011. Analysis on the impact of aerosol optical depth on surface solar radiation in the Shanghai megacity. China. Atmos. Chem. Phys. 11, 3281–3289.
Xu, H., Guo, J., Ceamanos, X., Roujean, J.L., Min, M., Carrer, D., 2016. On the influence of the diurnal variations of aerosol content to estimate direct aerosol radiative forcing using MODIS data. Atmos. Environ. 141, 186–196.
Yang, K., Wu, H., Qin, J., Lin, C., Tang, W., Chen, Y., 2014. Recent climate changes over the Tibetan Plateau and their impacts on energy and water cycle: A review. Global Planet. Change 112, 79–91.
Yang, X., Zhao, C., Luo, N., Zhao, W., Shi, W., Yan, X., 2020a. Evaluation and Comparison of Himawari-8 L2 V1.0, V2.1 and MODIS C6.1 aerosol products over Asia and the Oceania regions. Atmos. Environ. 220, 117068.
Yang, Y., Zheng, Z., Yin, S., Roth, M., Ren, G., Gao, Z., Wang, T., Li, Q., Shi, C., Ning, G., Li, Y., 2020b. $PM_{2.5}$ pollution modulates wintertime urban-heat-island intensity in the Beijing-Tianjin-Hebei Megalopolis, China. Geophys. Res. Lett. 47. https://doi.org/10.1029/2019GL084288.
Ye, D.Z., Chou, J.F., Liu, J.Y., 2000. Causes of sand-stormy weather in northern China and control measures. Acta Geo. Sci. 55, 513–521.
Yu, X., Cheng, T., Chen, J., Liu, Y., 2007. Climatology of aerosol radiative properties in northern China. Atmos. Res. 84, 132–141.
Zhang, J.H., Mao, J.T., Wang, M.H., 2002. Analysis of the aerosol extinction characteristics in different areas of China. Adv. Atmos. Sci. 19, 136–152.
Zhang, M., Ma, Y., Gong, W., Wang, L., Xia, X., Che, H., Hu, B., Liu, B., 2017a. Aerosol radiative effect in UV, VIS, NIR, and SW spectra under haze and high-humidity urban conditions. Atmos. Environ. 166, 9–21.
Zhang, T., Li, T., Yue, X., Yang, X., 2017b. Impacts of aerosol pollutant mitigation on lowland rice yields in China. Environ. Res. Lett. 12, 104003.
Zhang, P., et al., 2019a. Latest progress of the Chinese Meteorological Satellite Program and core data processing technologies. Adv. Atmos. Sci. 36, 1027–1045.
Zhang, Z., Wu, W., Fan, M., Tao, M., Wei, J., Jin, J., Tan, Y., Wang, Q., 2019b. Validation of Himawari-8 aerosol optical depth retrievals over China. Atmos. Environ. 199, 32–44.
Zhang, X., et al., 2020. The development and application of satellite remote sensing for atmospheric compositions in China. Atmos. Res. 245, 105056.
Zhao, B., Wang, Q., Mao, J., Qin, Y., 1983. Optical remote sensing atmospheric aerosol and water vapor. China Sci. D. 10, 951–962.
Zhao, F., Tan, Y., Li, Z., Gai, C., 2012. The effect and correction of aerosol forward scattering on retrieval of aerosol optical depth from Sun photometer measurements. Geophys. Res. Lett. 39.
Zhao, Z., Cao, J., Shen, Z., Xu, B., Zhu, C., Chen, L.W.A., Su, X., Liu, S., Han, Y., Wang, G., Ho, K., 2013. Aerosol particles at a high-altitude site on the Southeast Tibetan Plateau, China: Implications for pollution transport from South Asia. J. Geophys. Res. 118, 11,360–311,375.
Zhao, H., Che, H., Ma, Y., Xia, X., Wang, Y., Wang, P., Wu, X., 2015. Temporal variability of the visibility, particulate matter mass concentration and aerosol optical properties over an urban site in Northeast China. Atmos. Res. 166, 204–212.
Zhao, H., Che, H., Xia, X., Wang, Y., Wang, H., Wang, P., Ma, Y., Yang, H., Liu, Y., Wang, Y., Gui, K., Sun, T., Zheng, Y., Zhang, X., 2018. Multiyear ground-based measurements of aerosol optical properties and direct radiative effect over different surface types in Northeastern China. J. Geophys. Res. 123.
Zhao, H., Che, H., Gui, K., Ma, Y., Wang, Y., Wang, H., Zheng, Y., Zhang, X., 2020. Interdecadal variation in aerosol optical properties and their relationships to meteorological parameters over northeast China from 1980 to 2017. Chemosphere 247, 125737.
Zheng, Y., Che, H., Zhao, T., Zhao, H., Gui, K., Sun, T., An, L., Yu, J., Liu, C., Jiang, Y., Zhang, L., Wang, H., Wang, Y., Zhang, X., 2017a. Aerosol optical properties observation and its relationship to meteorological conditions and emission during the Chinese National Day and Spring Festival holiday in Beijing. Atmos. Res. 197, 188–200.
Zheng, Y., Che, H., Xia, X., Wang, Y., Wang, H., Wu, Y., Tao, J., Zhao, H., An, L., Li, L., Gui, K., Sun, T., Li, X., Sheng, Z., Liu, C., Yang, X., Liang, Y., Zhang, L., Liu, C., Kuang, X., Luo, S., You, Y., Zhang, X., 2019. Five-year observation of aerosol optical properties and its radiative effects to planetary boundary layer during air pollution episodes in North China: Intercomparison of a plain site and a mountainous site in Beijing. Sci. Total Environ. 674, 140–158.
Zhu, J., Xia, X., Che, H., Wang, J., Zhang, J., Duan, Y., 2016. Study of aerosol optical properties at Kunming in southwest China and long-range transport of biomass burning aerosols from North Burma. Atmos. Res. 169, 237–247.
Zhu, J., Xia, X., Wang, J., Che, H., Chen, H., Zhang, J., Xu, X., Levy, R., Oo, M., Holz, R., Ayoub, M., 2017. Evaluation of Aerosol Optical Depth and Aerosol Models from VIIRS Retrieval Algorithms over North China Plain. Remote Sens. 9, 432.
Zhu, J., Xia, X., Che, H., Wang, J., Cong, Z., Zhao, T., Kang, S., Zhang, X., Yu, X., Zhang, Y., 2019. Spatiotemporal variation of aerosol and potential long-range transport impact over the Tibetan Plateau. China. Atmos. Chem. Phys. 19, 14637–14656.